Neuron

CellPress

Primer

Voltage imaging: A practical guide

Adam E. Cohen[1,*] and Daozheng Gong[1]
[1]Departments of Chemistry and Chemical Biology, and Physics, Harvard University, Cambridge, MA 02138, USA
*Correspondence: cohen@chemistry.harvard.edu
https://doi.org/10.1016/j.neuron.2026.08.002

SUMMARY

Recent advances in genetically encoded voltage indicators (GEVIs), optical instrumentation, and analysis software have brought voltage imaging within reach of most neuroscience labs. Voltage imaging can resolve subthreshold dynamics and action potentials across scales, from the flickering of single ion channels to large-scale neural population dynamics in behaving animals. This primer provides a practical guide to the choices involved in setting up a voltage imaging experiment, including selecting a voltage indicator, choosing excitation wavelengths and microscopy configurations, expressing the constructs in the desired cell types, and extracting information from the data. We discuss the physical principles that govern signal-to-noise ratio, the trade-offs between one-photon and two-photon excitation, and the use of structured illumination to improve contrast in tissue. Our aim is to provide a reference for new and seasoned voltage imagers on how to design effective voltage imaging experiments.

INTRODUCTION: VOLTAGE IMAGING GOES MAINSTREAM

Our bodies buzz with electrical bursts. From action potentials in neurons to the membrane potential in mitochondria, cells use and modulate transmembrane potential to regulate signaling, transport, and metabolism. Every membrane-enclosed structure can support a membrane potential, and every protein and small molecule in the membrane feels the tug of the transmembrane electric field. Membrane potential is a key physiological variable in life, most famously in the nervous system, where it enables millisecond-timescale information processing, but also across tissues and species. For a review of the many factors that contribute to membrane voltage, see Cohen and Venkatachalam.[1]

Although membrane potential is ubiquitous and essential to life, it is also ephemeral. Voltage cannot be purified, sequenced, or run on a gel: it must be measured *in situ* and in live samples. Historically, this was first achieved via sharp electrodes, carefully inserted into cells,[2] and later by patch-clamp measurements, which, to this day, offer unrivaled accuracy and time resolution.[3] However, electrode-based measurements are technically challenging, low throughput, often impractical in moving samples, and lack spatial resolution.

Starting in the late 1960s, scientists sought to develop molecular contrast agents to convert membrane voltage into a fluorescence signal.[4–6] In the past 15 years, there have been major advances in genetically encoded voltage indicators (GEVIs) (reviewed in Xu et al.,[7] Adam,[8] Yang and St-Pierre,[9] St-Pierre et al.,[10] and Knöpfel and Song[11]), imaging instrumentation[12–26] (reviewed in Wang et al.[27]), and software for signal extraction and analysis (reviewed in Silva et al.[28]). Whereas voltage imaging has historically been a niche approach, the tools have matured to the point where this technique can be broadly practiced. Within the last year, there has been a flurry of publications that used voltage imaging to address neuroscience questions,[29–31] including publications from labs that do not specialize in tool development.

Voltage dynamics occur across a wide range of spatial and temporal scales and in diverse samples. There is no universally optimal voltage imaging approach. The key decisions to make concern (1) molecular reporter, (2) imaging instrumentation, and (3) data management, signal extraction, and analysis. Decisions along these three dimensions are intertwined.

This primer is meant as a practical guide. It covers the issues a researcher should consider when contemplating a voltage imaging experiment. This is not an exhaustive or historical overview, and the citations are illustrative rather than exhaustive. We begin by discussing the applications that motivate voltage imaging, then address the physical factors governing signal quality, followed by practical guidance on indicators, instrumentation, and data analysis.

WHEN TO DO A VOLTAGE IMAGING EXPERIMENT

Voltage imaging has been applied across scales of biological organization, from studies on individual heterologously expressed ion channels[32,33] and intracellular organelles[34] to studies in awake, behaving animals[14,35–37] (Figure 1).

Across these scales of organization, voltage imaging applications in neuroscience can be roughly classified by the type of information produced: (1) studying subcellular and single-cell physiology, i.e., how the molecular components of a cell govern its input-output properties; (2) mapping functional connections, i.e., how spikes in one neuron influence the voltage of its downstream partners; and (3) mapping network dynamics, i.e., the coordinated activity patterns across populations of neurons.

Single-cell and subcellular voltage dynamics

Neuronal membrane voltage is set by the combined activity of dozens of ion channel types, neurotransmitter receptors, and

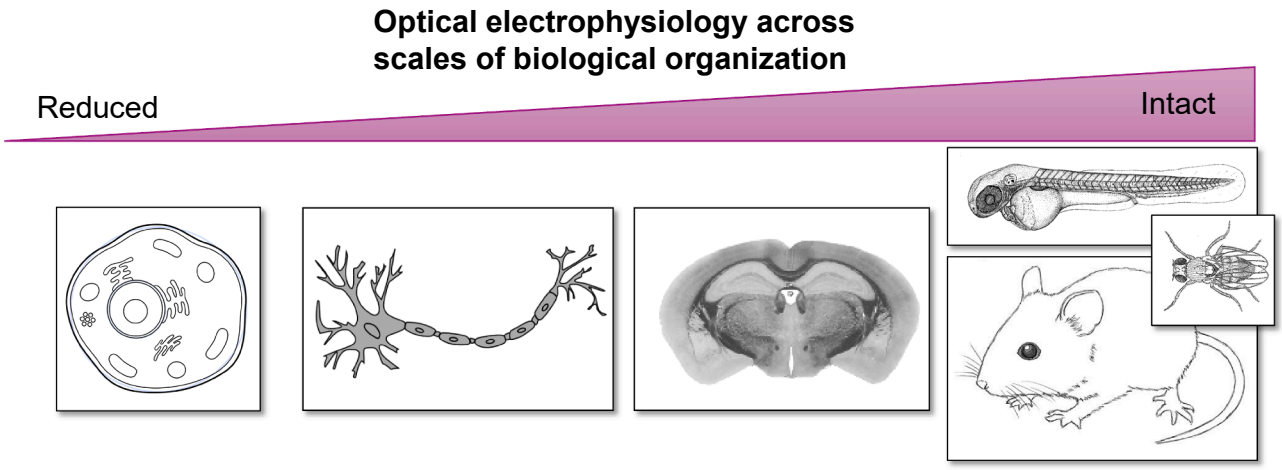

Ion channels	Cultured neurons	Slices	In vivo
Ion channel pharmacology[33,39]	Human iPSC-based disease modeling[40,41]	Dendritic integration[42]	Network dynamics (subthreshold and spiking) during behavior[29–31,43,44]
High-throughput target-based screens[39]	Organelle electrophysiology[34]	Mapping functional connectivity[46–48]	Learning and memory[49,51,52]
Organelle electrophysiology[34]	Functional phenotypic screens[13,38,41,45]	Mapping excitability[55]	Dendritic integration[53,56,57]
	Axonal physiology[54]		Worms[58], flies[59], fish[60,61]
	Synaptic physiology[50]		

Figure 1. Voltage imaging across scales

Example applications of voltage imaging, from pharmacological screens in heterologously expressed ion channels to studies of network dynamics in behaving animals.

References: Williams et al.[13,38]; Huang et al.[29]; Taxidis et al.[30]; Brown et al.[31]; Zhang et al.[33,39]; Saminathan et al.[34]; Kiskinis et al.[40]; Werley et al.[41]; Park et al.[42]; Haziza et al.[43]; Lowet et al.[44]; Liu et al.[45]; Csillag et al.[46]; Layous et al.;[47] Moya et al.[48]; Carolan et al.[49]; Fan et al.[50,51]; Gonzalez et al.[52,53]; Hoppa et al.[54]; Lou et al.[55]; Wong-Campos et al.[56]; Liao et al.[57]; Azimi Hashemi et al.[58]; Huang et al.[59]; Kawashima et al.[60]; Böhm et al.[61]

intracellular signaling pathways and is strongly influenced by neuronal geometry. The membrane voltage, which affects the gating of each channel type, depends on the currents through all channel types. This nonlinear cross-coupling between ion channels presents a challenge for determining the relative contributions of each channel type to the overall dynamics.

Patch-clamp measurements in "voltage-clamp" mode can decouple the contributions of each channel type to the total membrane current, but these measurements are technically demanding and lack spatial resolution. Though voltage imaging operates in "current-clamp" mode, one can nonetheless resolve the contributions of distinct channel types through combinations of voltage imaging, optogenetic stimulation, pharmacological or genetic perturbations, and computational modeling.[62]

Example applications of voltage imaging to single-cell electrophysiology include studies of gating and pharmacology of heterologously expressed sodium channels,[33,39] pharmacological and genetic screens to identify molecular modulators of neural excitability,[13,38,45,63] maps of dendritic integration and back-propagation in brain slices[42] and *in vivo*,[56] studies identifying determinants of spike propagation and waveform in axons,[54] maps of neuronal subtype-specific excitability during behavior,[64] and studies of excitability in neuronal models of disease.[38,40]

Many of these studies pair a blue-excited optogenetic actuator with a red-shifted voltage indicator for all-optical electrophysiology ("Optopatch").[65] Optogenetic stimulation allows one to probe neural input-output properties over a wider range of parameters, and in a more systematic fashion, than one can achieve through passive observation or sensory stimulation. Equipped with knowledge of local input-output properties, one can then observe these transformations at work in the context of physiological activity. This approach is analogous to how an electrical engineer uses a function generator and oscilloscope to dissect input-output properties of components embedded in a larger circuit.

Mapping synaptic and gap-junctional connectivity

A simplified view of neural function is that synaptic inputs combine to drive subthreshold voltage; when this voltage crosses a threshold, the neuron spikes. Within this view, the subthreshold voltages primarily reflect synaptic inputs, while spiking reflects the outputs. These input-output relationships were originally established through whole-cell patch-clamp recordings, which provide precise voltage measurements but are limited to one or two neurons at a time and require high technical skill. Voltage imaging can be useful to resolve synaptic (and gap-junctional) connections, either by correlating the subthreshold voltage in a postsynaptic cell with the spike times in a presynaptic cell or by optogenetically perturbing a presynaptic cell or population and recording the postsynaptic responses. These

approaches have been used in cultured neurons,[50] brain slices,[48] and *in vivo*.[49,51,66]

Synaptic inhibition is sometimes difficult to discern because the resting potential may be close to the reversal potential of the inhibitory ion channels ("shunting inhibition"). In this case, steady-state optogenetic depolarization of the postsynaptic neurons can increase the driving force for the inhibitory currents, unmasking their effect on membrane potential.[66]

Mapping network dynamics

Voltage imaging can map collective patterns of subthreshold dynamics, as well as precise spike timing and synchrony in neural populations. This approach has been used to map the dynamics of populations of identified neurons in the mouse hippocampus,[30,67] cortex,[36,67,68] and cerebellum,[31] as well as in zebrafish,[60,61] and for cortex-wide maps of ensemble-average membrane potential.[43] This approach may also be useful for deducing plasticity rules *in vivo*.

Although the above categories of experiments capture the neuroscience areas in which voltage imaging has been most often applied, creative researchers will certainly find other applications, such as recording from non-neuronal cell types,[69] recording from intracellular organelles,[34] and relating voltage dynamics to other molecular signals, such as calcium, glutamate, or neuromodulators.[46,48]

PLANNING A VOLTAGE IMAGING EXPERIMENT

Voltage signals are small and brief: ΔF/F per spike is typically ~10%–40%; (in some GEVIs, ΔF/F is negative for a depolarizing voltage step, and following convention, in discussions of signal-to-noise ratio [SNR] we use ΔF/F to indicate |ΔF/F|), and spike waveforms are approximately millisecond-long events—so experiment design requires attention to maximizing SNR while avoiding damage or unintentional perturbation to the tissue. Detailed analyses of the SNR in voltage imaging experiments are provided in Wilt et al.[70] and Brooks et al.[71] Here, we give some rules of thumb.

SNR

In a measurement that detects, on average, N photons, the discreteness of the photons leads to trial-to-trial variations of approximately $\sqrt{N}$. This "shot noise" is an unavoidable constraint on voltage imaging experiments. The shot noise-limited SNR of a voltage measurement is approximately

$$SNR = \frac{\Delta N}{\sqrt{N+B}}. \qquad \text{(Equation 1)}$$

Here, ΔN is the change in the number of detected photons associated with the event of interest, N is the baseline number of photons from the reporter in the absence of the event, and B is the number of "background" photons detected from other sources and mixed with the signal. Equation 1 is a best-case scenario, assuming no other noise sources.

Each parameter in Equation 1 is influenced by the GEVI properties (brightness, voltage sensitivity, response kinetics, and trafficking), the microscope design (optical sectioning and spatial and spectral filtering), and the analysis approaches (methods of pixel selection and weighting). This interplay illustrates how molecular, optical, and computational tools interact to determine the success of a voltage imaging experiment.

In the absence of background, the SNR scales as $SNR \approx \frac{\Delta N}{\sqrt{N}} = \frac{\Delta N}{N}\sqrt{N} = \frac{\Delta F}{F}\sqrt{N}$. Thus, voltage sensitivity $\left(\frac{\Delta F}{F}\right)$ contributes linearly to SNR, while photon count only contributes through its square root. The photon count N equals the count rate, Γ, times the event duration, τ (assuming measurement time and event duration are approximately matched). Thus, slower signals (e.g., postsynaptic potentials) can be measured more precisely than fast ones (e.g., gap-junction-mediated spikelets). The count rate also increases proportionally to the integration area. Thus, bigger sources (e.g., whole cells) can be measured more precisely than small sources (e.g., dendritic spines).

The required count rate to achieve a given SNR is:

$$\Gamma = \frac{(SNR)^2}{\left(\frac{\Delta F}{F}\right)^2 \tau}. \qquad \text{(Equation 2)}$$

For example, to resolve a change in fluorescence of ΔF/F = 1% (corresponding to a subthreshold fluctuation of a few mV for most modern GEVIs) with SNR = 5 requires detecting at least $N = 2.5 \times 10^5$ photons from the signal source. If one wishes to detect this event in τ = 1 ms, then one must detect photons at a rate $\Gamma = 2.5 \times 10^5$ photons/10^{-3} s = 2.5×10^8 photons/s. On the other hand, if one is principally focused on spike counting, one might have ΔF/F = 20%, target SNR = 5, and integration time τ = 3 ms (e.g., for a GEVI with an ~3-ms response time such as ASAP7y[72]). In this case, the count rate need only be 2.1×10^5 photons/s, more than 1,000-fold lower than the previous example.

For measurements *in vivo*, additional noise comes from breathing, blood flow, and motion artifacts. Although careful mounting and mechanical stabilization can mitigate these sources somewhat, these artifacts often need to be corrected in post-processing.

Choosing a target SNR

What is a good target SNR? The spike SNR—defined as the peak fluorescence change divided by the standard deviation of the baseline noise—sets the spike detection fidelity. Signal detection theory describes this relationship.[70] At each time bin, a spike-detection algorithm must determine whether a spike occurred. Each bin constitutes an independent statistical test, so the detection threshold must be set high enough that the false-positive rate remains well below the neuron's actual firing rate. For example, at a 1-kHz sampling rate, setting the spike-detection threshold high enough to limit false-positive detections to <0.1 per second leaves a detector with an SNR of 1 able to identify fewer than 1% of spikes. At SNR = 3, ~25% of spikes are detected; at SNR = 5, ~90% are detected; and at SNR ≥ 7, >99.9% are detected. Matched filtering against a known spike waveform can improve spike detection fidelity when the action potential is well sampled across multiple time bins, and temporal smoothing similarly enhances the detectability of subthreshold signals by a factor proportional to the square root of the number

of averaged bins. As a rule of thumb, SNR should be $\geq$5 for spike counting.

Limits on illumination

One can increase the SNR by increasing the illumination intensity, I, to a point. For one-photon (1P) excitation, the shot-noise-limited SNR scales as $SNR \propto I^{1/2}$. For experiments in live mouse brain, the optical limit can be set either by tissue heating or by photochemical toxicity. At wavelengths longer than ~560 nm, heating is typically the main concern, either via hemoglobin (Hb) absorption or direct water heating. The heating primarily depends on the total power delivered to the sample. For mouse brain, this power should be <~200 mW,[73] though if a laser is tightly focused, local heating can be a problem at lower intensity.[14,55] Intermittent measurement protocols can accommodate higher power because the tissue can cool between measurements. In zebrafish, brain slices, or cell culture, the maximum safe power can be much higher because only a small fraction of the incident light is absorbed.

Photochemical toxicity

Another limitation comes from photochemical toxicity. Optically excited chromophores can trigger a variety of redox reactions with toxic byproducts.[74] At wavelengths <~560 nm, the primary photosensitizers are endogenous chromophores: flavins, flavoproteins, and cytochromes. In fact, flavoproteins (excited at 420–490 nm; emission at 515–570 nm) are spectrally similar to green fluorescent protein (GFP) and show brain-activity-dependent changes in autofluorescence *in vivo*.[75] At longer wavelengths, endogenous phototoxicity is negligible, but the chromophore in the GEVI itself can mediate photodamage through side reactions from its optically excited state.[76] Photochemical damage is cumulative, so intermittent measurement protocols may not help. It is important to ensure that the functional properties of the system are not perturbed by the illumination, e.g., by (1) repeating measurements at different illumination intensities and (2) checking that the functional properties of the system are unchanged between the beginning and end of an experiment.

For small transparent animals such as zebrafish, one should also consider that bright illumination may reach the eyes and directly affect behavior.

Photobleaching

Photobleaching constrains the total duration of a voltage imaging experiment. With the most recent chemigenetic[77] and fully protein-based[78,79] GEVIs, recordings can be performed *in vivo* for many tens of minutes. Because photobleaching typically involves a redox reaction of the chromophore, photobleaching and phototoxicity often go hand in hand.

Photobleaching and phototoxicity are typically more of a concern for mapping subcellular voltage distributions than for whole-cell or network-level imaging, where each cell is treated as a single electrical compartment. To maintain constant SNR, the photon rate per signal source must be kept constant. When each signal source comprises a subcellular region, these photons must originate from a correspondingly small membrane area, requiring high local irradiance and hence greater photodamage per GEVI molecule. When one approximates a cell as a single compartment, the fluorescence can be distributed over the whole-cell membrane, with a correspondingly lower concentration of photochemical products.

Calibration

Voltage imaging typically reports relative fluorescence changes rather than absolute millivolt values and performs best for detecting events with durations between ~1 ms and ~1 s. On slower timescales, most samples show slow drifts in fluorescence due to photobleaching, sample motion, GEVI trafficking, or fluctuations within the light source. In some cases, calibration can be achieved by simultaneous patch-clamp recording, but this adds complexity and does not scale to large-scale recordings. Emerging techniques for absolute voltage imaging are described below under "Special-purpose GEVIs."

Choosing a wavelength

High-performance voltage indicators come in colors across the visible and near-infrared spectrum. In terms of photophysics (brightness and photostability) and sensing ($\Delta F/F$, response speed, and linearity), there are now good options at many wavelengths, and the list keeps growing. With hybrid chemigenetic indicators such as Voltron2[77] and Positron,[80] one can choose the color on the day of the experiment via the exogenously added HaloTag-ligand dye. Thus, the GEVIs themselves do not particularly constrain the choice of wavelength within the visible range.

In choosing a wavelength, the factors to consider are (1) availability of high-power and stable light sources, (2) optical properties of the tissue, and (3) compatibility of the GEVI with additional optogenetic actuators or fluorescent reporters. Factors (2) and (3) generally favor red or far-red GEVIs.

Light sources

Historically, voltage imaging required lasers, but thanks to improvements in GEVI brightness and advances in LED technology, high-quality voltage imaging *in vivo* or *in vitro* is now possible with LEDs. High-power and stable LEDs developed for the video projector market have peak wavelengths around 470, 530, and 615 nm. With good heat-sinking (and active cooling in demanding applications), these LEDs can produce many watts of stable optical power. For studying micron-scale structures, it can be desirable to focus the light tightly, in which case lasers are still preferable. Comparatively inexpensive and high-power diode lasers are available at 532 and 635 nm. We have also performed voltage imaging using more expensive but still high-quality lasers at 488, 561, 594, and 607 nm. Thus, for 1P voltage imaging, availability of suitable light sources is not much of a constraint.

Optical properties of brain tissue: Redder is better

Figure 2 shows the six physical processes involving light transport in tissue that are relevant to voltage imaging. In brain tissue, autofluorescence is 136-fold lower at 640 nm than at 488 nm.[55] Photochemical toxicity in cultured cells is >100-fold lower at 640 nm than at 488 nm.[74] The greatest concern for imaging red GEVIs in tissue is photothermal heating. At 640 nm, optical absorption of brain tissue, and hence light-induced heating, is ~20-fold lower than at 488 nm, and 3- to 5-fold lower than in

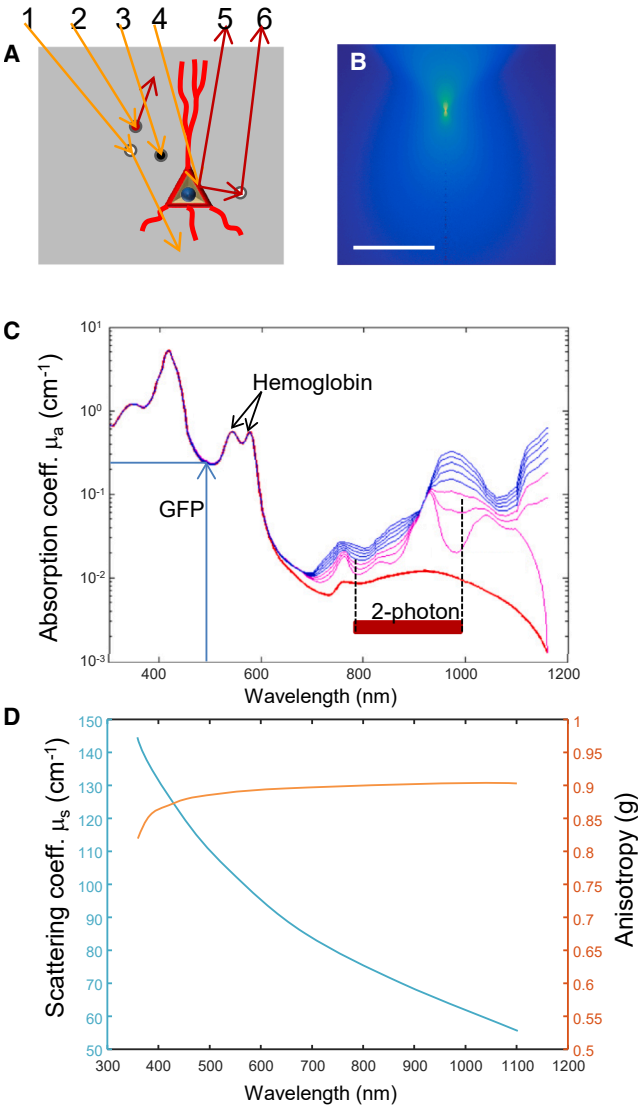

Figure 2. Light propagation in brain tissue

(A) Physical processes relevant to light propagation in a voltage imaging experiment. (1) Scattering of excitation. (2) Out-of-focus fluorescence, from either tissue autofluorescence or out-of-focus GEVIs. (3) Absorption, leading to heating or phototoxicity and attenuation of the excitation light. (4) In-focus GEVI excitation and (5) fluorescence (this is the signal!). (6) Scattering of GEVI fluorescence.

(B) Numerical simulation of a focused light beam (λ = 640 nm) in brain tissue, showing the presence of a sharp focus surrounded by a halo of scattered light. Scale bar: 100 μm.

(C) Model of brain tissue absorption spectrum. The blue to pink lines correspond to increasing fat content. Adapted from Jacques.[81]

(D) Optical scattering length (blue) and anisotropy (orange) in brain tissue. Adapted from Yaroslavsky et al.[82]

the 800–1,000 nm band used for most two-photon (2P) imaging.[81] The absorption of Hb drops sharply at wavelengths > 600 nm. At 640 nm, the absorption coefficients of Hb and oxyHb are 27% and 2%, respectively, of their values at 488 nm.

The maximum tissue depth for a voltage imaging experiment is usually set by light scattering. When light passes through tissue, the rays are deviated by local inhomogeneities in the refractive index. Photons in brain tissue are likely to scatter many times before they are absorbed: a comparison of Figures 2C and 2D shows that across most of the visible spectrum, absorption coefficients (the inverse of the absorption length) range from 0.01 to 1 cm^{-1}, while scattering coefficients range from 70 to 120 cm^{-1}. This is why you can observe light from a flashlight through your hand (particularly the red light) but you cannot resolve much internal structure. Optical scattering lengths in brain tissue are ~50% longer at 640 nm than at 488 nm, enabling correspondingly deeper imaging.[82]

Another important parameter of light scattering in tissue is the scattering anisotropy, g. This is a measure of how much each scattering event deviates the light (it is the average cosine of the scattering angle). As g approaches 1, the deviations from scattering become small; at $g = 0$, a scattered photon is equally likely to go in any direction. In brain tissue, $g \sim 0.9$, so scattering only slightly deflects photon paths. This means that light can be partially focused and images can be formed at depths several-fold greater than the scattering length. Figure 2B shows a numerical simulation of a focused laser beam in brain tissue. The light forms a sharp focus, surrounded by a haze of scattered light. This spatial profile of light scattering has important implications for the design of voltage imaging experiments, as discussed below.

Multimodal imaging or Optopatch: Redder is better

As discussed above, the pairing of functional imaging with patterned optogenetic stimulation greatly facilitates exploration of neural circuits. To combine stimulation and measurement, the actuator and reporter must be spectrally orthogonal. Although there exist red-shifted channelrhodopsin variants, all retain 20%–30% activation at blue wavelengths.[83] In contrast, red-shifted GEVIs can be paired with blue-shifted channelrhodopsins, such as CheRiff, with negligible optical crosstalk.[42,65] Due to the high intensity requirements of voltage imaging, even slight channelrhodopsin activation by the red light source can drive spurious opsin activation. We observed this crosstalk in CheRiff even when exciting a voltage indicator at 561 nm.[84] GEVI excitation should be at 594 nm or longer wavelengths to avoid crosstalk with channelrhodopsins.

Red-shifted GEVIs also enable simultaneous imaging with GFP-based reporters, such as the GCaMP family calcium indicators[85] or the iGluSnfr[86,87] glutamate indicators. Given that most fluorescent reporters are excited on the blue end of the spectrum, there is more flexibility in pairing a red-shifted voltage indicator with a blue-shifted molecular reporter than vice versa.

In our lab, these considerations have largely tilted the balance in favor of redder GEVIs. Most of our recent voltage imaging work has been with Voltron2, loaded with the brain-permeant HaloTag Ligand dye JF608. For illumination, we use either a 607-nm laser or a red LED designed for video projector applications.

When to go green: Subthreshold sensitivity or 2P imaging

Green-emitting GEVIs such as the ASAP family (up to ASAP7[72] at the time of writing), JEDI-2P,[23] and FORCE1s[88] offer distinct

Please cite this article in press as: Cohen and Gong, Voltage imaging: A practical guide, Neuron (2026), https://doi.org/10.1016/j.neuron.2026.08.002

Box 1. GEVI performance metrics

Voltage sensitivity measures the steady-state relation between voltage and fluorescence. It is often reported as $\Delta F/F_0$ per 100 mV (typically assuming F_0 is measured at −70 mV). However, many GEVIs show greater sensitivity near the neuronal resting potential (∼−70 mV) than at more positive voltages, so you should check the F vs. V curve to ensure suitability for your purpose. The denominator, F_0, is sensitive to measurement and analysis conditions: it is increased by intracellular GEVI molecules, which do not contribute to voltage sensitivity, and by fluorescent background, e.g., in tissue. Some analyses define F_0 and ΔF via a whole-cell average, while others select them from well-trafficked membrane regions; some subtract background, whereas others do not. As a result, reported values of $\Delta F/F_0$ can vary widely for a given GEVI. Also note that for some opsin-based GEVIs, the voltage sensitivity depends on the intensity and wavelength of the illumination. There are both positive-going and negative-going GEVIs; the sign of $\Delta F/F_0$ makes little practical difference.

Response kinetics measures the time course of the fluorescence response to a step change in membrane voltage. They are often reported as a $\tau_{1/2}$ or an exponential time constant. Faster responses more faithfully convert voltage waveforms into fluorescence; this is critical for recording from neurons with very narrow spikes, such as parvalbumin-positive (PV) interneurons. Response kinetics can be different between the voltage upstroke and downstroke; for applications focused on spike counting at relatively low spike rates, one may wish for a fast response to the spike upstroke and a slower recovery to maximize the number of photons, ΔN, detected per spike. As with voltage sensitivity, response kinetics depend on measurement and analysis conditions. Many GEVIs show multi-exponential kinetics, so sometimes "fast" and "slow" time constants are reported separately, along with their relative amplitudes. Though rarely reported, kinetics can also depend on the starting and ending membrane potential in a voltage step (just as time constants of ion channel gating variables depend on voltage). GEVI kinetics can depend steeply on temperature, often being several-fold faster at 37°C than at room temperature. For most applications, a submillisecond response time is desirable. Response kinetics also interact with imaging strategy[91]: with pulsed or scanned illumination, a fast indicator may rise and return to baseline between exposures, causing some events to be missed, whereas a slower indicator effectively integrates over time, which can be advantageous for detecting spikes but may blur fast dynamics.

Effective brightness measures the rate of photon detection per signal source. This parameter depends on photophysical properties (optical extinction coefficient and fluorescence quantum yield), protein properties (expression level and membrane trafficking), and instrumentation (excitation wavelength and intensity; fluorescence collection efficiency). Because the protein expression level can vary substantially between preparations, it is hard to generalize from published results. In general, higher expression is better, though GEVI overexpression can disrupt neuronal electrophysiology, e.g., inducing transient jumps to a depolarized state. Brighter illumination is also better, up until photobleaching, heating, or phototoxicity become a problem. Sometimes brightness is defined solely in terms of per-molecule photophysical properties (extinction coefficient × quantum yield), but here we include all parameters that contribute to the rate of photon detection.

Photostability measures the rate at which signal is lost due to irreversible photobleaching of the GEVI molecules. The rate of photobleaching often scales as a nonlinear function of illumination intensity, I^{α}, with $\alpha > 1$, and also depends on local oxygen concentration. For these reasons, photobleaching rates can vary.

Subcellular localization is particularly important for applications of GEVIs in tissue. To record from many neurons concurrently, one usually wishes for soma-localized GEVIs. Soma targeting can be achieved via C-terminal fusion of a $K_V2.1$ motif, as described below, and is usually denoted with a "som" prefix or an "ST" suffix (these are equivalent). To map subcellular distributions of voltage in dendrites and/or axons, one wishes for a broadly trafficked GEVI. In all cases, one wants the GEVI to traffic as efficiently as possible to the cell membrane to avoid contamination from intracellular sources.

Single-spike SNR is a useful practical measure that integrates all experimental factors that contribute to a voltage imaging experiment.

advantages, including large ΔF/F, compatibility with standard GFP filter sets and light sources, full genetic encoding without requiring exogenous dyes, and excellent 2P performance. Though these indicators have a slower response compared with opsin-based GEVIs, this can be advantageous in terms of maximizing the total change in detected photons, ΔN, for spike counting. For newcomers with existing GFP-optimized setups, or for applications where simplicity and large signals are paramount, green GEVIs can be the better choice.

CHOOSING A GEVI

There is rapid and accelerating progress in GEVI engineering. Any list of the best-available GEVIs will be obsolete by the time this primer is published. Furthermore, GEVI performance is often context specific (e.g., because of variations in membrane trafficking), and the choice will depend on many experiment-specific factors. To guide users, we are releasing, alongside this primer, a website that allows the ranking and comparison of GEVIs across multiple performance metrics (https://gevibench.org/). This website is periodically updated by an automated AI agent.

Comprehensive charts comparing GEVI performance have been published recently.[89,90] Several recent reviews cover GEVI design.[7,11] Here, we focus on the classes that are showing widespread adoption in neuroscience beyond the labs of their developers. We discuss the important parameters for different experimental contexts. Box 1 describes some of the important characteristics of a GEVI.

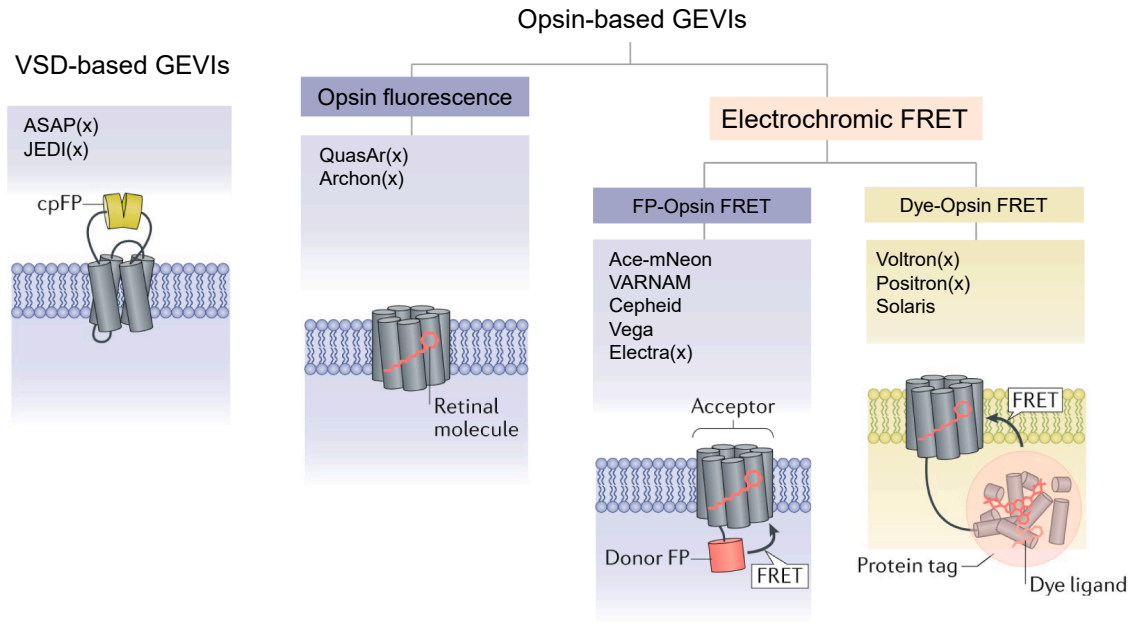

Figure 3. Classes of broadly used GEVIs

(A) Coupling of a voltage-sensitive domain (VSD) to a circularly permuted fluorescent protein (cpFP) modulates the cpFP fluorescence.

(B–D) (B) In some microbial rhodopsins, voltage-dependent protonation of the retinal modulates the near-infrared retinal fluorescence. Voltage-dependent changes in the retinal absorption spectrum can modulate fluorescence resonance energy transfer (FRET) from an appended (C) fluorescent protein or (D) chemogenetic tag, modulating the brightness of the appended fluorescent moiety. Adapted from Knöpfel and Song.[11]

Broadly, state-of-the-art GEVIs fall into two main classes (Figure 3): voltage-sensitive domain (VSD)-based GEVIs convert changes in membrane voltage into a mechanical rearrangement of one or more fluorescent proteins, modulating the fluorescence. Opsin-based GEVIs use voltage-dependent protonation of a retinal cofactor in a microbial rhodopsin to modulate either the direct retinal fluorescence or the fluorescence of an appended fluorescent tag.

VSD-based GEVIs

The leading VSD-based GEVIs use a VSD from the sea squirt *Ciona intestinalis*, with a circularly permuted fluorescent protein fused between the S3 and S4 transmembrane helices on the extracellular face. The best-performing indicators in this class are derived from the ASAP voltage indicators,[92] with ASAP6[93] and ASAP7[72] variants recently reported. Building on the ASAP scaffold, indicators optimized for 2P voltage imaging are also available: JEDI-2P,[23] a slow variant; FORCE1s,[88] optimized for spike counting at low photon-detection rate; and JEDI-2Psub,[49] a variant optimized for subthreshold imaging. The ASAP and related indicators are spectrally similar to GFP. These indicators have excellent subthreshold sensitivity and are compatible with 2P imaging but are not as fast or photostable as some of the opsin-based GEVIs.

Opsin-based GEVIs

Our lab discovered that the endogenous fluorescence of microbial rhodopsin-based proton pumps was sensitive to membrane voltage, first in *E. coli*[94] and then in mammalian cells.[95] Engineered variants of GEVIs based on Archaerhodopsin 3 (Arch) include the Archon family[36,96] and QuasArs,[14,65] currently up to QuasAr6.[97] Fluorescence of the retinal chromophore in microbial rhodopsins is excited at 630–640 nm, emits in the near-infrared region (peak around 710 nm), and is exquisitely photostable, fast, and voltage sensitive. However, this fluorescence is 50- to 100-fold dimmer than GFP, requiring intense laser illumination and presenting a challenge for imaging in tissue.

FRET-opsin GEVIs

In the opsin-based GEVIs, voltage controls the absorption spectrum of the retinal cofactor.[98] In the FRET-opsin GEVIs, this change in absorption modulates the efficiency with which the retinal quenches the fluorescence of an appended fluorescent tag.[99] Unquenched tag fluorescence is detected as the voltage-dependent signal. This "electrochromic fluorescence resonance energy transfer (FRET)" approach has been dramatically improved via fusions to ever-more-stable and -bright fluorescent proteins (Ace-mNeon[35] and Ace-mNeon2,[68] ElectraON and ElectraOFF,[79] and Vega[78]). Opsins have also been fused with red-shifted fluorescent proteins,[68,100,101] permitting simultaneous multicolor voltage imaging in distinct neural populations. However, the red shift via this approach (excitation at 561 nm) was not sufficient to avoid spurious excitation of the red edge of channelrhodopsins expressed in the same cells.

Further improvements in brightness, photostability, and spectral tunability came from replacing the attached fluorescent protein with a chemogenetic indicator based on the HaloTag scaffold. The non-fluorescent HaloTag receptor becomes

fluorescent upon covalent labeling with an organic dye bearing a chloroalkane linker. The Voltron[37] indicator and its improved variant Voltron2[77] can be loaded with dyes with excitation wavelengths from 488 to 615 nm. We recently found that the dye JF608-HaloTag ligand is readily bioavailable (crosses the blood-brain barrier and cell membranes *in vivo*), maintains good voltage sensitivity, and is excited by either 594- or 607-nm lasers or bright red video-projector LEDs at 615 nm. These conditions offer favorable tissue optics and are compatible with crosstalk-free optogenetic stimulation *in vivo*.[102] Engineering of the opsin scaffold to switch the Schiff base accessibility from the intracellular face to the extracellular face converted Voltron into a positive-going indicator, Positron.[80]

The requirement for HaloTag-ligand dyes can be an additional expense and inconvenience. Fortunately, the Janelia Research Campus provides these dyes to academic research groups upon request. Experiments in cell culture require minuscule dye doses. Experiments in live adult mice typically require an entire vial comprising ~100 nmol of dye, delivered via retro-orbital injection. The background dye clears from the brain within ~12 h, and the labeled opsins can be recorded for up to ~1 week before another dye injection is required. Local intracranial dye injection through a silicone window has also been demonstrated and uses much less dye.[103]

A longstanding mystery of the FRET-opsin GEVIs is that they appeared to lose voltage sensitivity under 2P illumination.[104] A recently introduced FRET-opsin GEVI termed "2Photron" showed 2P voltage sensitivity and could be used for simultaneous 2P voltage and calcium imaging *in vivo*.[105] We recently determined that in Voltron1 and Voltron2, the loss of 2P voltage sensitivity occurs because the dark-adapted state is not sensitive to voltage.[106] At the start of a 1P voltage imaging experiment, the illumination quickly populates this voltage-sensitive state, whereas in 2P voltage imaging, each molecule is only illuminated transiently and intermittently, never building up a population in the voltage-sensitive state. 2P illumination schemes that revisit the same molecules every few milliseconds can achieve voltage sensitivity with these GEVIs.

This observation also implies that, even under 1P excitation, the light must be sufficiently intense to populate the voltage-sensitive intermediate state. For Voltron2-JF608, excited at 594 nm, this threshold is approximately 400 mW/cm^2.[107] Fortunately, most neural recording experiments use 10-fold higher intensity, but for organ-wide or time-lapse voltage imaging experiments, one might be tempted to use lower intensity and then be surprised to find that the voltage sensitivity has gone away.

Finally, one must remember that all opsin-based GEVIs require a retinal cofactor. For experiments in rodents or zebrafish *in vivo*, and with mammalian cells grown in serum, there is typically sufficient ambient retinal to load the GEVIs. For experiments with human induced pluripotent stem cell (hiPSC)-derived neurons grown in defined media, it may be necessary to supplement the medium with all-*trans* retinal prior to the experiment.[40] *Drosophila*[108] and *C. elegans*[58] must also be fed all-*trans* retinal because they lack sufficient endogenous retinal synthesis. If an opsin-based GEVI seems not to be working, it is worth trying to supplement all-*trans* retinal. Otherwise, the problem may be with membrane trafficking.

Trafficking is key

The efficiency of trafficking to the plasma membrane and the subcellular distribution within the membrane are key determinants of the success of a voltage imaging experiment. Separation of intracellular from surface signals in post-processing is technically demanding and only feasible for high-magnification imaging. Unfortunately, the efficiency of membrane trafficking can be context specific. For example, QuasAr2 worked well in cultured neurons[65] but did not traffic to the cell membrane *in vivo*.[14] Trafficking efficiency depends not just on the transmembrane components but also on appended tags. For example, the presence of a fluorescent protein expression tag on the QuasAr and Archon GEVIs helps substantially with trafficking, for reasons that are not understood.

Subcellular localization

To map circuit function, one may wish to express a voltage indicator in many closely spaced cells. However, if the GEVI enters the dendrites and axons too, then the cell-body "meatballs" are completely lost in the neuropil "spaghetti" (Figure 4A). To see why this is such a severe issue for voltage indicators, one must consider the surface-to-volume ratio of different neuronal compartments. In CNS neurons, the ratio of soma surface area to axo-dendritic surface area is ~1:20.[109,110] Thus, with a well-trafficked and densely expressed GEVI, 95% of the fluorescence comes from optically unresolvable neuropil. In contrast, the ratio of soma volume to axo-dendritic volume is ~3:2. For a soluble Ca^{2+} indicator, somatic Ca^{2+} signals can be resolved even when the calcium indicator is in the neuropil too.

This problem can be mitigated by localizing the GEVI to the soma membrane and excluding it from the dendrites. We showed that C-terminal fusion of a GEVI to the soma-localization motif from the K_V2.1 potassium channel[111,112] substantially restricts expression to the soma and proximal dendrites[14] (Figure 4B). The same motif has been shown to soma-localize channelrhodopsins, which can be helpful for cell-targeted optogenetic stimulation.[113]

To study dendritic integration, one would like sparsely expressing cells and efficient trafficking throughout the dendritic arbor. We found that an N-terminal Lucy-Rho tag[114] facilitates trafficking of Voltron2 throughout the dendrites and axons of pyramidal cells *in vivo*.[42,102]

Special-purpose GEVIs

Several GEVIs have been developed with properties tailored for specific uses. A longstanding challenge has been to measure absolute as opposed to relative changes in membrane voltage. The indicator rEstus[115] addresses this challenge via a ratiometric measurement of the fluorescence of a red fluorescent protein, mKate2, appended to a variant of ASAP3. However, ratiometric measurements are susceptible to differential rates of chromophore maturation and photobleaching and nonuniformities in illumination intensity. An alternative strategy is to convert voltage into a time-domain signal, which can be measured with absolute accuracy. This approach is the basis for techniques based on the electronic excited-state lifetime.[104,116] A third method probed absolute voltage via voltage-dependent changes in the kinetics of the Arch photocycle.[117]

Please cite this article in press as: Cohen and Gong, Voltage imaging: A practical guide, Neuron (2026), https://doi.org/10.1016/j.neuron.2026.08.002

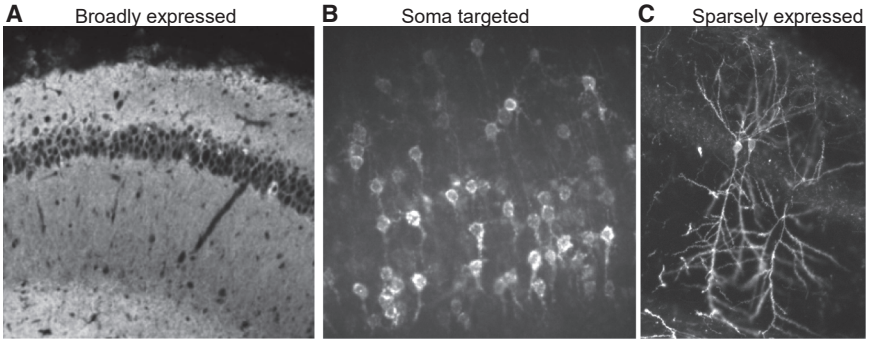

Figure 4. Control of expression and trafficking is crucial in tissue

(A) In a densely expressed and well-trafficked GEVI, cell bodies are lost amid the neuropil.[14]

(B) Soma localization via a $K_V2.1$ soma-targeting (ST) motif enables dense expression in tissue (here Voltron2-ST in cortex).

(C) Dendrite trafficking via a Lucy-Rho (LR) motif enables dendrite imaging, but only if the expression is very sparse (here LR-Voltron2 in hippocampus).

The complex photocycles of microbial rhodopsins present many possibilities for engineering useful voltage-sensing capabilities. For example, in the GEVIs paQuasAr3[14] and NovArch,[106] blue light converts the GEVI from a non-fluorescent to a red-fluorescent and voltage-sensitive state, enabling targeted voltage imaging at the intersection of red and blue laser beams. Other Arch mutants undergo voltage-dependent equilibria during illumination, which are then preserved in the dark.[118] These tools, in principle, enable a temporal separation between the encoding of electrical activity and a subsequent readout. Approaches based on these ideas have been dubbed "flash memory" and "light-gated integrator," but these tools have not been refined by protein engineering or widely used.

Other GEVIs have been targeted to intracellular organelles. A GEVI derived from ArcLight, termed Aahn, was targeted to the endoplasmic reticulum.[119] Though not genetically encoded, DNA-based voltage indicators have been targeted to endocytic organelles and the *trans*-Golgi network.[34] A GEVI targeted to the mitochondrial inner membrane would be a powerful tool for tracking metabolic state, but such a GEVI has not yet been developed.

MICROSCOPY

Historically, voltage imaging has had a reputation as a technically demanding method, the domain of "optics jocks." Although there are highly sophisticated instruments for certain applications, advances in GEVIs, instrumentation, and software have made voltage imaging accessible to most neuroscience labs. A recent review of microscopy for voltage imaging is in Wang et al.[27] There is a wide range of technical approaches, with no universally "best" strategy. Below we outline the trade-offs in technical performance, cost, and complexity.

Low-cost options

For 1P voltage imaging in cultured neurons (primary or iPSC-derived), one can assemble a high-performance setup on any epifluorescence microscope for a relatively low cost. Inverted microscopes are convenient for imaging cultured cells, because the top of the dish is then easily accessible for perfusing drugs, but upright dipping objectives can be used too.

For the ASAP-family or FRET-opsin GEVIs, one can use a high-power LED as the light source. The illumination intensity at the sample should be 2–8 W/cm^2. For the Arch-based GEVIs, one needs a red (630–640 nm) laser, with an intensity at the sample of 50–500 W/cm^2. In either case, with a good objective (numerical aperture [NA] > 0.7, 20×, or 60×) and a camera that can run at >500 Hz, one will be able to detect spikes from single neurons.

With most CMOS cameras, the maximum frame rate scales inversely with the number of rows, so voltage imaging requires restricting the field of view (FOV) to a strip. Although high-end scientific CMOS cameras offer the best performance, these typically cost >$20,000; at a modest decrease in SNR, one can use cameras that cost <$2,000, run over a USB3 connection, and still image spikes and subthreshold voltages in cultured neurons.

When using a red-excited GEVI (either Arch-based or Voltron2 with JF594 or JF608), one can then use blue light for optogenetic stimulation or for simultaneous imaging of a green fluorescent reporter, e.g., of calcium or glutamate. A blue LED can either be coupled through the same excitation port as the red light or—for experiments in cell culture—illuminate the sample from the side opposite the red source, avoiding the cost of a beam-combining dichroic and a dual-wavelength imaging dichroic.

The fpbase website (fpbase.org) is extremely helpful in selecting combinations of light sources, chromophores, and filters that will work well together. The optobase website (optobase.org) has similar information on light-activated protein-based switches and dimerizers.

Structured illumination for voltage imaging in tissue

The main challenges for 1P voltage imaging in tissue come from light scatter and background. Photons in brain tissue typically scatter many times before they are absorbed, so absorption events happen in a broadly distributed volume.[81] Some of the out-of-focus photons excite fluorescence, which leads to a diffuse background. Thus, one wants to minimize the total amount of light that enters the sample. Excitation photons that intersect the cell membrane contribute to useful signal, while those that pass through interstitial regions only contribute to background. Restricting illumination to the signal-generating parts of the sample is essential for achieving a high SNR (Figure 5). A review of light-patterning technologies in the context of targeted optogenetics can be found in Ronzitti et al.[120]; the same principles apply to targeted-illumination voltage imaging.

Targeted illumination (either 1P or 2P) faces a trade-off between illumination confinement and robustness to motion: the tighter the confinement of the illumination to the nanometers-thick cell

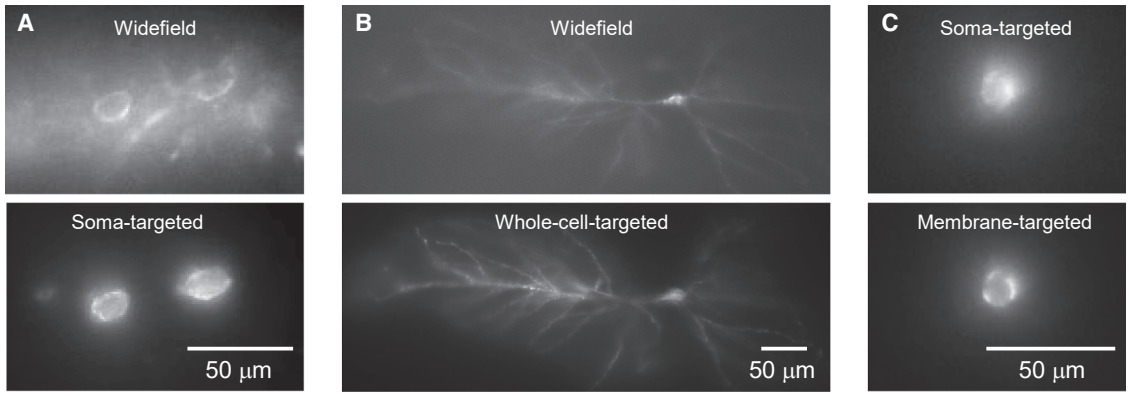

Figure 5. Optical targeting improves contrast in tissue

(A and B) Comparison of wide-field (top) vs. DMD-patterned targeted illumination (bottom) in (A) CA1 oriens layer, *in vivo*, and (B) a broadly expressing CA1 pyramidal neuron in acute slice.

(C) Comparison of DMD-patterned soma-targeted illumination (top) vs. SLM-patterned illumination targeted to the equatorial membrane in an L1 interneuron (bottom).

membrane, the more susceptible the signal is to sample motion. Differential imaging[23] and active feedback[53] approaches have been used to minimize motion artifacts in 2P imaging. In 1P voltage imaging, motion is usually handled in post-processing[14]—active image stabilization has not yet been implemented.

For 1P voltage imaging from only one or a few cells that are closely spaced, one can simply use a field-stop iris (i.e., an iris in the excitation path that is re-imaged onto the sample) to restrict the incident light to the region of interest. This simple step can increase signal-to-background ratio in tissue by a factor of ~10.[106]

To record from more broadly separated sources or extended objects (e.g., a dendritic tree), it is necessary to pattern the light to target only the signal-bearing parts of the sample. With LED illumination, this is best done with a digital micromirror device (DMD). The DMD is the core element of most video projectors. It contains a microfabricated array of millions of mirrors, which can be electrostatically switched between "on" and "off" states at >10 kHz. In a video projector, each DMD pixel corresponds to one pixel in the image. When coupled to a microscope, each DMD pixel controls the illumination at a corresponding microscopic spot in the sample. A single DMD chip can be used to pattern both red light for targeted illumination voltage imaging and blue light for targeted optogenetic stimulation.

The optical path from DMD to sample is analogous to the optical path from sample to wide-field camera; only the directions of the light rays are reversed. Thus, DMD systems are simple to set up. The main limitation of DMDs is that they are optically inefficient: dark pixels direct incident light into a beam dump. DMD systems face a trade-off between illuminated FOV and peak intensity.

Though a few DMD modules with integrated optics are commercially available, none is explicitly optimized to provide the high light intensities needed for voltage imaging. To date, voltage imaging with structured illumination requires either specially configuring a commercial module or constructing one around commercially available DMD driver electronics.

Liquid crystal spatial light modulators (SLMs) are an alternative to DMDs for targeted-illumination voltage imaging with laser light.[25,121] SLMs are usually placed in a Fourier plane and redirect the light, though they can also be placed in an image plane and used as an amplitude mask for direct point-to-point mapping. An SLM can direct all the light on its face to a single focus (or multiple foci) to create targeted zones of high-intensity light. Open-source designs for SLM-based illumination systems have been published.[122]

The chief advantages of DMD-based systems are (1) DMDs are much faster (>10 kHz vs. typically <500 Hz for SLMs); (2) DMDs are achromatic: they work equally well across the visible spectrum, whereas SLMs must be calibrated for each wavelength; (3) DMDs have a direct point-to-point mapping onto the sample, whereas SLMs require complex algorithms to compute the optimal diffraction pattern for a given target illumination intensity; and (4) DMDs work with LEDs or lasers, whereas SLMs work only with lasers. The chief advantages of SLMs are that (1) the SLM can bring light to a sharp focus, e.g., illuminating only the equatorial edge of a cell, where the fluorescence signal is brightest, and (2) SLMs can create complex three-dimensional focal patterns. In general, DMDs are better if one wants patterned illumination over a substantial fraction of a sample, while SLMs are better for highly focal illumination of a few points. After having tried DMD- and SLM-based systems in our lab, we prefer DMDs for most applications.

Ultra-wide-field voltage imaging

The number of simultaneously recorded neurons, M, is a useful figure of merit for a voltage imaging system. The data throughput scales proportionally to M, and the number of possible connections scales as M^2. In most families of microscope objectives, there is a trade-off between FOV and light-collection efficiency: lower-magnification objectives tend to have lower NA. Typically NA $\geq$ 0.5 is needed for voltage imaging, which restricts the magnification to >10×. There exist very large "mesoscope" objective lenses, which have NA $\geq$ 0.5 and ~2× magnification. These objectives, when coupled with sufficiently bright light sources and large-format filters and optics, allow kHz frame-rate voltage imaging over FOVs as large as 5 mm. With wide-field

illumination, these systems can be used for all-optical electrophysiology from thousands of cultured neurons (primary or hiPSC-derived neurons) simultaneously.[12,13,41] When combined with DMD-based targeted illumination in an upright geometry, the same system can be used for high-throughput optical electrophysiology in brain slices or *in vivo*.

Engineered excitation and emission light fields

The structured illumination systems described above controlled the spatial distribution of the light entering the sample and used simple wide-field collection to capture the emission. Additional improvements can be achieved by engineering the angular distribution and polarization of the light field in the excitation and emission paths. In the "targeted illumination confocal" approach, a vertical light sheet is swept across a DMD face and then re-imaged onto the sample.[123] A slit in the detection path partially rejects out-of-focus light. This hybrid approach outperforms either targeted illumination or slit confocal alone. Similarly, a hybrid of DMD-patterned structured illumination and spinning disk confocal also outperformed either modality alone.[124] For many GEVIs, the chromophore is partially oriented in the cell membrane. By controlling the polarization of the excitation light, one can achieve a modest improvement in signal level with no increase in background or optical power.[21]

Light-sheet microscopy confines the illumination to a thin plane, so out-of-focus regions receive minimal light. In the classical configuration, the light sheet enters from the side. For transparent samples such as zebrafish and worms, this approach enables high-resolution and photon-efficient volumetric voltage imaging.[60,61,125] A recently developed high-speed remote focusing module substantially increased the speed and efficiency of volumetric light-sheet voltage imaging.[126] Single-objective light-sheet approaches have also been developed,[127] though the increased path length of an oblique light-sheet propagating through tissue leads to transverse scattering, which partially counteracts the benefits of light-sheet optical sectioning.

A variety of other geometries have also been applied to 1P voltage imaging. These include spinning disk,[85] high-speed multiplane confocal,[16] SLM in the emission path,[128] and light-field[129] systems. Recently, several custom light-field approaches have been optimized to achieve simultaneously high speed and high background rejection for volumetric voltage imaging in tissue.[18,103] Systems that combine light-field detection and patterned illumination are likely to achieve further advances in signal quality and imaging depth.

A particularly ingenious voltage imaging system achieved wide-field fluorescence lifetime imaging (FLIM) by using a pulsed epifluorescence light source in combination with a synchronously modulated electro-optic (EO) modulator in the emission path ("EO-FLIM").[20] The FLIM signal is insensitive to photobleaching or sample motion, allowing robust measurement of voltage signals in moving samples.

Software for 1P voltage imaging

Voltage imaging experiments often require integration of light-patterning devices (DMDs, SLMs, or galvos), imaging devices (cameras or photomultipliers), and sensory stimulation or behavioral monitoring instruments. The high frame rates and requirements for microsecond-level synchronization distinguish voltage imaging from other neurophysiology experiments (e.g., 2P Ca^{2+} imaging). We developed a source-available non-commercial software package, Luminos, that implements these capabilities and is compatible with virtual reality experiments.[130] The Luminos software provides automatic spatial and temporal registration of light-patterning and imaging, so specific features in the image can be optically highlighted or stimulated.

2P voltage imaging

2P microscopy can achieve background-free measurements to greater depth and with higher spatial resolution than is possible with 1P imaging. Due to the high intensity required for nonlinear 2P excitation, 2P voltage imaging is always performed with ultrafast (~100 fs) pulsed lasers and with focused illumination. The key design parameters are the repetition rate, shape, and targeting of the laser pulses.

Acousto-optical scanning 2P systems use diffraction in special nonlinear crystals to provide inertia-free random-access beam steering in three dimensions.[131–134] These systems can typically visit ~40,000 points/s, targeted to cell membranes and avoiding non-informative interstitial regions. Although the number of simultaneously recorded sources is limited to ~40 at 1 kHz, the recorded points can be rapidly reconfigured to build up data over a larger population. Acousto-optical 2P scanning has recently been used in several projects to map dendritic voltages *in vivo*, taking advantage of the high spatial resolution and 3D random-access targeting.[53,72]

An alternative approach uses a resonator cavity to split a single laser pulse into a set of laterally[135,136] or axially[137] offset pulses. Provided that the time delays between pulses exceed the fluorescence excited-state lifetime (typically ~4 ns), the signals from each pulse can be resolved by a high-speed detector. These spot-multiplier techniques thereby enable sampling at a higher voxel rate than could be achieved by point-scanning alone. The FACED 2.0 technique recently demonstrated simultaneous spike-resolved recording from up to ~200 neurons *in vivo* at a depth of ~140 μm[135] (a depth also accessible to 1P imaging), and a recent preprint reported spike-resolved recording of 165 neurons at a depth of 490 μm.[136] A beam multiplexing strategy was also integrated into a head-mounted mini-scope, allowing 2P voltage imaging in freely behaving mice.[138]

Future directions in 2P voltage imaging

At present, 2P voltage imaging systems employ either random-access targeting of individual somata or pulse splitting with simple raster scanning. An opportunity for further advancement is to combine pulse splitting—to maximize the temporal information rate—with membrane-targeted illumination patterns or adaptive excitation[139] that avoid depositing non-useful laser pulses into the sample.

1P vs. 2P

The choice of the best imaging modality depends on the location of the signal sources and on the nature of the anticipated data. Broadly, 1P excitation provides ~10^3- to 10^4-fold more fluorescence per unit optical power into the sample,[71] enabling imaging

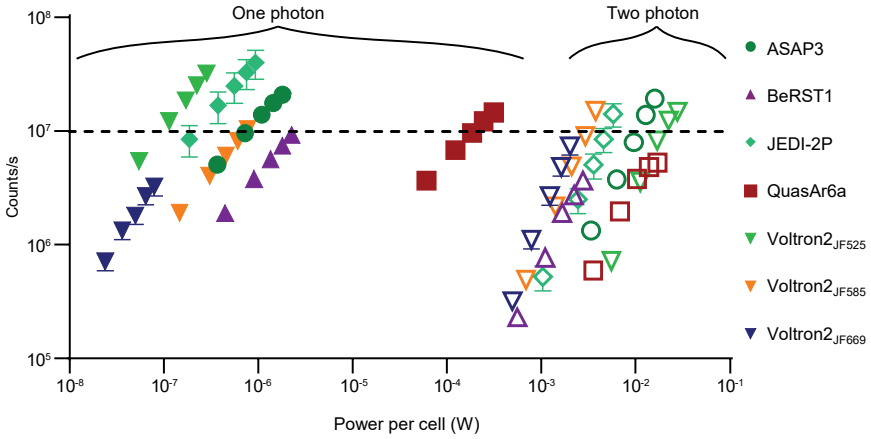

Figure 6. Comparison of signal levels under 1P and 2P excitation

Fluorescence counts as a function of power-per-cell under cell-targeted 1P imaging or rapid point-scanning 2P imaging with an 80 MHz laser. For both 1P and 2P, the wavelength was tuned to the excitation maximum. 1P data: filled symbols; 2P data: empty symbols. Error bars are SEM from at least $n = 8$ cells. The excitation wavelengths used for 1P (2P) excitation of each of the reporters were ASAP3 488 nm (930 nm), BeRST1 635 nm (850 nm), JEDI-2P 488 nm (930 nm), QuasAr6a 635 nm (900 nm), Voltron2$_{525}$ 488 nm (930 nm), Voltron2$_{585}$ 594 nm (1100 nm), and Voltron2$_{669}$ 635 nm (1220 nm). Figure adapted from Brooks et al.[71]

over wider areas and at faster rates (Figure 6), whereas 2P excitation offers greater depth penetration, better spatial resolution, and background-free detection. We recently compared the signal and noise properties of 1P vs. 2P voltage imaging in detail.[71]

Speed and throughput

In 1P imaging, the pixel rate is set by camera readout speed. For example, the Teledyne Kinetix22 camera reads 6.4×10^8 pixels/s in 16-bit mode or 3.8×10^9 pixels/s in 8-bit mode. In 2P imaging, the voxel rate is fundamentally limited by the fluorophore excited-state lifetime to 2–3 $\times$ 10^8 voxels/s. This order-of-magnitude difference in throughput means that 2P voltage imaging faces a more stringent trade-off between temporal resolution and the number of simultaneously measured sources. However, neither modality currently provides useful information at the raw sampling rate: one must accumulate sufficient photons to achieve the target SNR, as described above. In the photon-limited regime, 1P excitation provides a higher data rate than 2P.

Cost

One-photon voltage imaging can be performed with relatively inexpensive lasers (<$10,000) or very inexpensive LEDs (<$1,000); the most costly element is typically the high-speed camera ($25–$30,000). In contrast, the pulsed laser and customized scanning systems for 2P voltage imaging cost many hundreds of thousands of dollars.

Depth and resolution

In rodent brain tissue, light scattering limits 1P voltage imaging to a depth of 250–300 μm.[17] 2P voltage imaging can penetrate to ~700 μm[136,139] and provides superior spatial resolution and optical sectioning but at the cost of the speed and brightness constraints described above.

Practical guidance

For sparse sources within the top ~250 μm of tissue, 1P imaging is usually preferable: it delivers more photon counts per unit of delivered power, which is important for resolving small or rapid subthreshold events. For densely labeled samples or greater depths, 2P imaging becomes advantageous because it eliminates the out-of-focus background that degrades 1P recordings. 2P excitation is also valuable when three-dimensional targeting is required, as in some dendritic imaging experiments. For multi-neuron recordings, the 2P approach is currently best suited to spike counting, where photon-flux requirements are lower than for resolving subthreshold dynamics. 2P excitation is also often paired with GEVIs engineered for a slightly slower post-spike return to baseline; this increases the number of signal photons per spike (ΔN) and relaxes demands on the scanning apparatus at the cost of distorted spike waveforms.

DATA

Acquisition

Voltage imaging experiments can generate huge datasets; a researcher should plan for this at the outset. Modern scientific CMOS cameras can produce up to ~3 GB of data/s. The control computer must have the bandwidth to accept these data. Typically, this means either streaming to a RAM drive or to an array of two or more solid-state drives (SSDs), configured in a RAID0 configuration to maximize speed. One must also plan for long-term data storage. A good day of data taking can generate several TB of raw data.

The quantity of useful information in a voltage imaging movie is far less than the number of recorded pixels, because voltage dynamics are typically correlated between neighboring pixels, and many pixels are not on signal sources. A variety of compression algorithms have been developed,[140,141] but none yet runs in real time.

Figure 7 shows a typical voltage imaging analysis pipeline. See Silva et al.[28] for a comparative review of voltage imaging analysis pipelines. When analyzing a new voltage imaging dataset, it is essential to visualize the data after every analysis step, because datasets often have idiosyncratic features that can lead to unexpected results. We have developed a suite of simple MATLAB functions that facilitate exploratory analysis of voltage imaging data (Box 2).

Denoising

There are several sources of noise that can contaminate a voltage imaging movie. Movies *in vivo* often have some residual motion, particularly if the animal is awake, but even *in vitro*

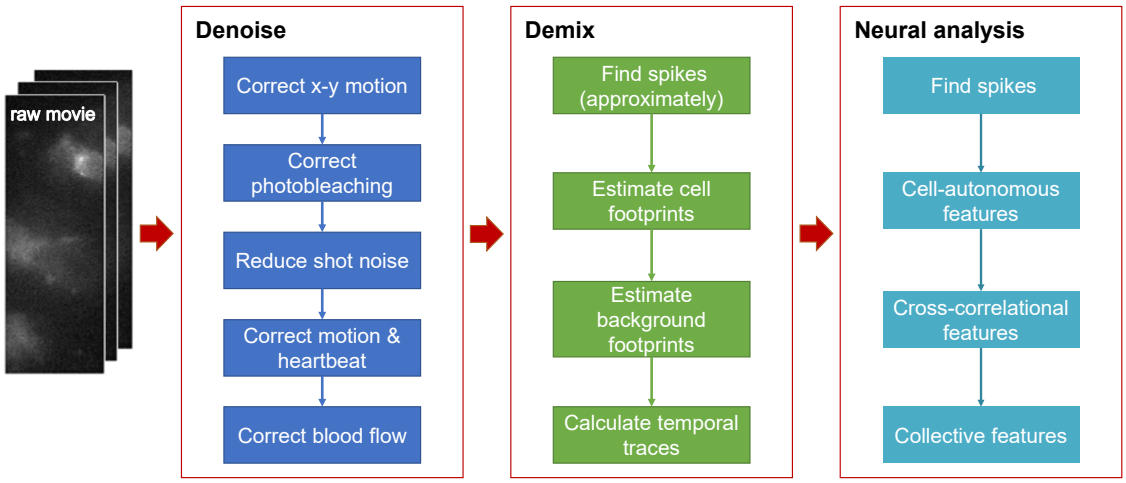

Figure 7. Voltage imaging data analysis
The primary steps comprise denoising the data, demixing (to separate signals from distinct sources), and analyzing the resulting traces.

movies can have sample drift, particularly if the movie is long. Lateral sample motion can be corrected by correlation-based algorithms such as NoRMCorre.[142] If the motions are small compared with the size of features in the image, one can perform computationally efficient motion correction by using the approximation $F(x+\Delta x, y+\Delta y) - F(x,y) \approx \frac{\partial F}{\partial x}\Delta x + \frac{\partial F}{\partial y}\Delta y$. By computing the gradient images $\frac{\partial F}{\partial x}$ and $\frac{\partial F}{\partial y}$, one can use a simple linear regression to solve for Δx and Δy relative to a reference image at each time step. To correct z-motion, one can pre-acquire a set of static snapshots at a series of small axial displacements from the focal plane. By cross-correlating each voltage image to each of these snapshots, one can also infer Δz. Because sample motion is usually slow compared with the kHz frame rate of voltage imaging, one need not calculate motion on every frame—one can calculate at intervals and then interpolate or calculate at every frame and smooth the results over several frames to achieve more accurate motion estimates.

Photobleaching is a common feature of voltage imaging movies. Often, the photobleaching rate varies across the image and/or follows a non-exponential decay. To accommodate these features, it is often useful to estimate the photobleaching time course pixel by pixel by temporally low-pass filtering the data. However, if there are slow changes in subthreshold voltage or spike rate, one does not want these to leak into the photobleaching estimate! It is thus often helpful to filter with a sliding ordinal filter (e.g., at the 10^{th} percentile for a positive-going GEVI) to avoid contamination from spikes. If there are known epochs where the true baseline voltage shifts (e.g., due to optogenetic or sensory stimulation), one can restrict the fitting to the unperturbed epochs and then interpolate the fluorescence baseline during the perturbations.

Shot noise is an unavoidable feature of all voltage imaging movies. The key feature of shot noise is that its value is uncorrelated between pixels and between frames, whereas most real voltage signals have finite extent in space and time. The variance of the shot noise is proportional to the mean intensity. The technique of penalized matrix decomposition (PMD) uses this difference in statistical properties to "denoise" voltage imaging movies.[140] Machine learning-based approaches are also tackling this problem.[143]

In exploratory analysis of a voltage imaging movie, one often wishes to know which parts of the movie show dynamics and which are static. This can be hard to discern by eye. One can define a ΔF movie by $\Delta F(t) = F(t) - \langle F \rangle_t$, where $\langle F \rangle_t$ indicates the time average. Sometimes, watching the ΔF movie reveals the active regions. It is tempting to attempt to make a map of the active regions by calculating the variance of the intensity at each pixel, i.e., $\sigma^2 = \langle \Delta F^2 \rangle_t$. However, due to the presence of shot noise, the σ^2 image ends up looking very much like F; i.e., brighter regions of the movie have more variance regardless of electrical activity. To map intensity fluctuations without contamination from shot noise, one can instead calculate the lag-1 covariance: $g^2(dt) = \langle \Delta F(t) \cdot \Delta F(t+dt) \rangle_t$, where dt is the interframe interval. This quantity is immune to shot noise because shot noise is uncorrelated between successive frames. Similarly, one could also correlate $\Delta F(t)$ with $\Delta F(t)$ shifted over by one pixel, again using the independence of shot noise between pixels.

Finally, *in vivo* measurements are often contaminated by heartbeat and breathing artifacts and blood flow. Static fluorescence signals (e.g., from autofluorescent puncta or improperly trafficked GEVI molecules) can be used to estimate these global contamination signals. Linear regression can then be used to remove these from the signal at each pixel. Signals from blood vessels typically need to be masked or locally filtered.

Demixing

A voltage imaging movie can often be represented as a sum of images of individual sources (e.g., cells), each modulated with its distinct temporal waveform. There is also often some background (e.g., from out-of-focus cells), which one wishes to separate from the signal. The purpose of demixing is to identify the individual source "footprints" and their corresponding temporal waveforms. Figure 8 shows that this can be expressed as a

Box 2. Useful functions for exploratory analysis of voltage imaging data

Here, we provide several MATLAB functions that we have found useful. These functions are available at https://github.com/adamcohenlab/Matlab-functions-for-Voltage-imaging-a-practical-guide.git.

clicky: the user manually defines one or more regions of interest (ROIs) in a voltage imaging movie. The function extracts and plots the mean intensity as a function of time in each region.

apply_clicky: applies ROIs defined in a clicky operation to a new movie. This enables reuse of ROIs across datasets.

clicky_PCA: performs principal component analysis (PCA) on each manually defined ROI in a movie. This can be useful for separating voltage signals from motion artifacts or background fluctuations.

lag1_image: calculates the lag-1 autocovariance of an image. It provides a map of where fluorescence fluctuations are occurring that is not biased by shot noise.

SeeResiduals: uses linear regression to remove from a movie one or more temporal waveforms. Each template waveform is scaled for a best-fit pixel by pixel to the movie, and then subtracted. The function returns a residual movie and maps of fitting coefficients. This is useful for correcting photobleaching, drift, and motion artifacts, as well as for identifying small signals that are overlaid by bigger signals.

matrix factorization problem, often known as "blind-source separation." There are many approaches to this problem, including independent components analysis (ICA),[144] non-negative matrix factorization,[141,145] and the recently introduced activity localization imaging.[146] When preparing data for any of these approaches, one can use the fact that neural spiking is typically less correlated between sources than are subthreshold potentials. Thus, by either high-pass filtering the data and/or selectively analyzing the time intervals around spikes, one can identify clean single-cell spatial footprints. One can then apply the pseudo-inverse of these spatial footprints to the original movie to extract the full time traces, including subthreshold dynamics.

Neural analysis

Once a voltage imaging movie has been denoised and demixed, the neuroscience fun begins. These analyses are typically customized for each experiment, but a few common steps are often useful. After spike finding, one often wishes to calculate a spike-triggered average movie of membrane potential in the triggering cell and in possibly connected cells. One can then examine spike-triggered average waveforms (e.g., to detect postsynaptic potentials). One can also calculate event-triggered average movies and waveforms, triggered by optogenetic stimuli, sensory inputs, or behavioral outputs. Beyond pairwise statistics, there is a rich and ever-growing toolbox for analyzing high-dimensional neural data.[147–149] Key differences from other modalities (e.g., neuropixels recordings, Ca^{2+} imaging) are that in voltage imaging data, one has access to subthreshold as well as spiking data, and the statistical structures and information content of these two data streams may be very different. Also, the ability to pair spatially and genetically targeted optogenetic stimulation with voltage imaging can reveal local single-cell and microcircuit input-output properties, which then inform models of responses to naturalistic inputs.

THE FUTURE OF VOLTAGE IMAGING

Voltage imaging is not a single technique—it is an integration challenge. The success of an experiment depends on the joint performance of the molecular reporter, the optical instrumentation, and the analysis pipeline. Each shapes the SNR, the susceptibility to artifact, and the class of biological questions that can be addressed. There is no universally "best" tool but rather a diverse toolbox from which one should judiciously select a reporter, optics, and computation to reveal the desired biology. Nonetheless, the field evolves rapidly, and newer tools can be strictly superior to older ones in the same class; staying current with the literature and performing rigorous side-by-side comparisons remain essential.

Voltage imaging is exquisitely sensitive, but with sensitivity comes sensitivity to artifact. Motion, blood flow, hemodynamic fluctuations, photobleaching, background fluorescence, and perturbations induced by the measurement itself can all masquerade as physiology, particularly as subthreshold voltages. Especially *in vivo*, one must take care not to confuse vascular or motion-related signals with local electrical events. Careful controls, validation across illumination conditions, and visualization of the spatial and temporal structures of the data at each analysis step are essential parts of the experimental design; these should not be afterthoughts.

MOLECULAR REPORTERS

For molecular reporters, there are exciting opportunities for the protein engineer. First, most measurements still report relative changes in fluorescence rather than absolute membrane voltage. Absolute voltage measurements would reveal mechanistic details inaccessible to current techniques and may be particularly important in dendrites, non-spiking cells such as astrocytes, and organelles. Second, the membrane voltage reflects the combined action of many underlying conductances. Strategies to resolve the individual contributions, e.g., by probing absolute voltage and membrane conductance or by combining voltage imaging with channel-selective modulation, would carry additional information. Strategies to pair voltage imaging with reporters of neurotransmitters, neuromodulators, or signaling pathways would connect bioelectrical signaling to the upstream causes and downstream effects. Third, subcellular and organellar electrophysiology remain under-explored. Improved targeting, trafficking, brightness, and photostability will be needed to

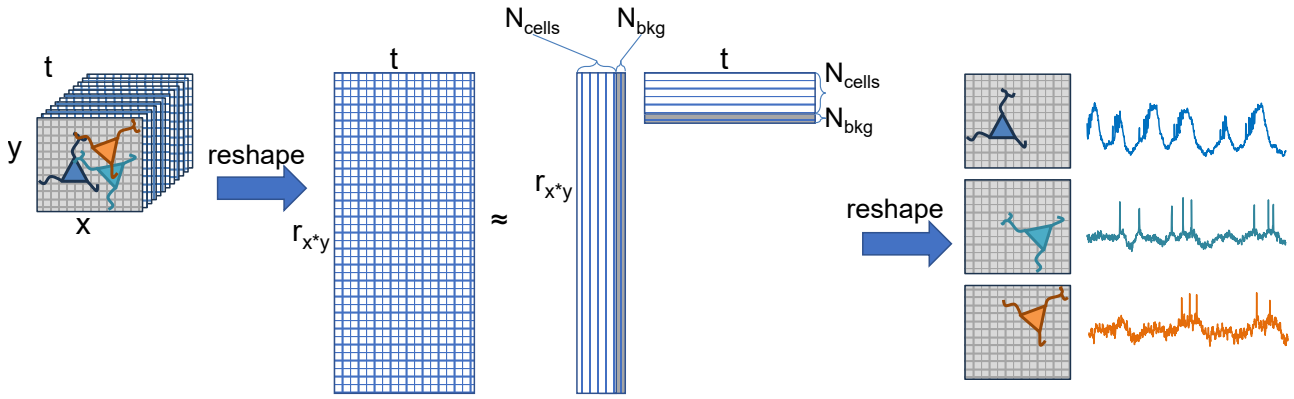

Figure 8. Voltage imaging demixing

A voltage imaging movie can be represented as a three-dimensional array, with two space dimensions and one time dimension. This array can be reshaped into a matrix with one (large) space dimension and a time dimension. The demixing problem comprises representing the spatiotemporal data as a product of low-dimensional matrices of cell "footprints" and cell "time traces," plus one or more background terms.

map voltage in axons, spines, and intracellular membranes such as mitochondria and vesicles. Structures that are inaccessible to patch clamp, by virtue of size or location, require special consideration for how to calibrate putative voltage indicators and how to rule out the influence of spurious covariates such as pH or ionic strength.

INSTRUMENTS

In optical instrumentation, a major opportunity lies in further engineering of the excitation and detection light fields. Adaptive optics, targeted illumination, light-field imaging, and related approaches should help improve contrast and signal recovery in scattering tissue. Recent live tissue-clearing techniques[150] may also help break through the haze of tissue scattering. There is also a need for ultra-wide-field systems that retain optical sectioning and collection efficiency so that voltage imaging can scale to larger populations without sacrificing signal quality.

COMPUTATION AND ANALYSIS

In computation and analysis, the most immediate need is for automated and reliable signal extraction: denoising, demixing, artifact rejection, and event finding. These tools will be essential for making voltage imaging broadly accessible and for keeping pace with the scale of the datasets. Further ahead, real-time analysis may enable closed-loop experiments in which optogenetic or sensory perturbations are triggered by identified voltage patterns. Voltage imaging analysis pipelines should also support increasingly mechanistic model fitting, from conductance-based descriptions of dendritic integration to coarse-grained models of circuit and population dynamics.

MULTIMODAL INTEGRATION

A particularly exciting future direction is integration with complementary structural and molecular measurements. Post hoc spatial transcriptomics, connectomics, proteomics, and ultrastructural analysis may link voltage dynamics to cell identity, connectivity, molecular state, and local context. Likewise, multimodal functional measurements may connect voltage to neurotransmitter release, neuromodulation, intracellular signaling, and metabolism. In this sense, voltage imaging is evolving from a specialized measurement into a general framework for linking molecular mechanisms to electrical function across scales.

Our main message is that voltage imaging is already powerful, but its full impact will come from thoughtful integration. The field will benefit from continued diversification of tools; better coordination among molecular, optical, and computational approaches; and a culture of careful validation that treats physiological fidelity and artifact rejection as core scientific criteria.

ACKNOWLEDGMENTS

We thank all members of the Cohen lab for contributing to the research described in this primer and for reviewing this manuscript. This work was supported by the Gordon and Betty Moore Foundation; Schmidt Futures; Chan Zuckerberg Initiative Dynamic Imaging grant 2023-321177; a Brain Research Foundation Scientific Innovations Award BRF-SIA2022-02; NIH grants R01-NS126043, R01-NS133755, and R01-MH117042; Vannevar Bush Faculty Fellowship N0001418-1-2859; NSF Quantum Sensing for Biophysics and Bioengineering (QuBBE); and Quantum Leap Challenge Institute (QLCI) grant OMA-2121044.

DECLARATION OF INTERESTS

A.E.C. is a founder of Luminos Microscopy, which sells voltage imaging mesoscopes, and a consultant to Quiver Biosciences, Exin Therapeutics, and Morphoceuticals. A.E.C. holds multiple patents and is on multiple patent applications related to voltage imaging.

DECLARATION OF GENERATIVE AI AND AI-ASSISTED TECHNOLOGIES IN THE WRITING PROCESS

During the preparation of this work, the authors used ChatGPT to review the discussion. The authors take full responsibility for the content of the published article.

REFERENCES

1. Cohen, A.E., and Venkatachalam, V. (2014). Bringing bioelectricity to light. Annu. Rev. Biophys. *43*, 211–232. https://doi.org/10.1146/annurev-biophys-051013-022717.

2. Verkhratsky, A., Krishtal, O.A., and Petersen, O.H. (2006). From Galvani to patch clamp: the development of electrophysiology. Pflugers Arch. *453*, 233–247. https://doi.org/10.1007/s00424-006-0169-z.

3. Hille, B. (2001). Ion Channels of Excitable Membranes (Sinauer).

4. Tasaki, I., Watanabe, A., Sandlin, R., and Carnay, L. (1968). Changes in fluorescence, turbidity, and birefringence associated with nerve excitation. Proc. Natl. Acad. Sci. USA *61*, 883–888. https://doi.org/10.1073/pnas.61.3.883.

5. Cohen, L.B., Salzberg, B.M., Davila, H.V., Ross, W.N., Landowne, D., Waggoner, A.S., and Wang, C.H. (1974). Changes in axon fluorescence during activity: molecular probes of membrane potential. J. Membr. Biol. *19*, 1–36. https://doi.org/10.1007/BF01869968.

6. Cohen, L.B., and Salzberg, B.M. (1978). Optical Measurement of Membrane Potential (Springer).

7. Xu, Y., Zou, P., and Cohen, A.E. (2017). Voltage imaging with genetically encoded indicators. Curr. Opin. Chem. Biol. *39*, 1–10. https://doi.org/10.1016/j.cbpa.2017.04.005.

8. Adam, Y. (2021). All-optical electrophysiology in behaving animals. J. Neurosci. Methods *353*, 109101. https://doi.org/10.1016/j.jneumeth.2021.109101.

9. Yang, H.H., and St-Pierre, F. (2016). Genetically Encoded Voltage Indicators: Opportunities and Challenges. J. Neurosci. *36*, 9977–9989. https://doi.org/10.1523/JNEUROSCI.1095-16.2016.

10. St-Pierre, F., Chavarha, M., and Lin, M.Z. (2015). Designs and sensing mechanisms of genetically encoded fluorescent voltage indicators. Curr. Opin. Chem. Biol. *27*, 31–38. https://doi.org/10.1016/j.cbpa.2015.05.003.

11. Knöpfel, T., and Song, C. (2019). Optical voltage imaging in neurons: moving from technology development to practical tool. Nat. Rev. Neurosci. *20*, 719–727. https://doi.org/10.1038/s41583-019-0231-4.

12. Werley, C.A., Chien, M.-P., and Cohen, A.E. (2017). Ultrawidefield microscope for high-speed fluorescence imaging and targeted optogenetic stimulation. Biomed. Opt. Express *8*, 5794–5813. https://doi.org/10.1364/BOE.8.005794.

13. Williams, L.A., Joshi, V., Murphy, M., Ferrante, J., Werley, C.A., Brookings, T., McManus, O., Grosse, J., Davies, C.H., and Dempsey, G.T. (2019). Scalable Measurements of Intrinsic Excitability in Human iPS Cell-Derived Excitatory Neurons Using All-Optical Electrophysiology. Neurochem. Res. *44*, 714–725. https://doi.org/10.1007/s11064-018-2694-5.

14. Adam, Y., Kim, J.J., Lou, S., Zhao, Y., Xie, M.E., Brinks, D., Wu, H., Mostajo-Radji, M.A., Kheifets, S., Parot, V., et al. (2019). Voltage imaging and optogenetics reveal behaviour-dependent changes in hippocampal dynamics. Nature *569*, 413–417. https://doi.org/10.1038/s41586-019-1166-7.

15. Nguyen, T.N., Shalaby, R.A., Lee, E., Kim, S.S., Kim, Y.R., Kim, S., Je, H.S., Kwon, H.-S., and Chung, E. (2025). Ultrafast optical imaging techniques for exploring rapid neuronal dynamics. Neurophotonics *12*, S14608. https://doi.org/10.1117/1.NPh.12.S1.S14608.

16. Weber, T.D., Moya, M.V., Kılıç, K., Mertz, J., and Economo, M.N. (2023). High-speed multiplane confocal microscopy for voltage imaging in densely labeled neuronal populations. Nat. Neurosci. *26*, 1642–1650. https://doi.org/10.1038/s41593-023-01408-2.

17. Xiao, S., Cunningham, W.J., Kondabolu, K., Lowet, E., Moya, M.V., Mount, R., Ravasio, C., Economo, M.N., Han, X., and Mertz, J. (2024). In vivo voltage imaging with targeted illumination confocal (TICO) microscopy. In Neural Imaging and Sensing (SPIE), pp. PC1282804. https://doi.org/10.1117/12.3000992.

18. Wang, Z., Zhao, R., Wagenaar, D.A., Espino, D., Sheintuch, L., Benshlomo, O., Kang, W., Zhu, E., Lee, C.K., Schmidt, W.C., et al. (2025). Kilohertz volumetric imaging of in vivo dynamics using squeezed light field microscopy. Nat. Methods *22*, 2194–2204. https://doi.org/10.1038/s41592-025-02843-8.

19. Guo, R., Yang, Q., Chang, A.S., Hu, G., Greene, J., Gabel, C.V., You, S., and Tian, L. (2024). EventLFM: event camera integrated Fourier light field microscopy for ultrafast 3D imaging. Light Sci. Appl. *13*, 144. https://doi.org/10.1038/s41377-024-01502-5.

20. Bowman, A.J., Huang, C., Schnitzer, M.J., and Kasevich, M.A. (2023). Wide-field fluorescence lifetime imaging of neuron spiking and subthreshold activity in vivo. Science *380*, 1270–1275. https://doi.org/10.1126/science.adf9725.

21. Bloxham, B., Brinks, D., Kheifets, S., and Cohen, A.E. (2021). Linearly polarized excitation enhances signals from fluorescent voltage indicators. Biophys. J. *120*, 5333–5342. https://doi.org/10.1016/j.bpj.2021.10.028.

22. Nguyen, C., Upadhyay, H., Murphy, M., Borja, G., Rozsahegyi, E.J., Barnett, A., Brookings, T., McManus, O.B., and Werley, C.A. (2019). Simultaneous voltage and calcium imaging and optogenetic stimulation with high sensitivity and a wide field of view. Biomed. Opt. Express *10*, 789–806. https://doi.org/10.1364/BOE.10.000789.

23. Liu, Z., Lu, X., Villette, V., Gou, Y., Colbert, K.L., Lai, S., Guan, S., Land, M.A., Lee, J., Assefa, T., et al. (2022). Sustained deep-tissue voltage recording using a fast indicator evolved for two-photon microscopy. Cell *185*, 3408–3425.e29. https://doi.org/10.1016/j.cell.2022.07.013.

24. Chamberland, S., Yang, H.H., Pan, M.M., Evans, S.W., Guan, S., Chavarha, M., Yang, Y., Salesse, C., Wu, H., Wu, J.C., et al. (2017). Fast two-photon imaging of subcellular voltage dynamics in neuronal tissue with genetically encoded indicators. eLife *6*, e25690. https://doi.org/10.7554/elife.25690.

25. Tanese, D., Weng, J.-Y., Zampini, V., De Sars, V., Canepari, M., Rozsa, B.J., Emiliani, V., and Zecevic, D. (2017). Imaging membrane potential changes from dendritic spines using computer-generated holography. Neurophotonics *4*, 031211. https://doi.org/10.1117/1.NPh.4.3.031211.

26. Sims, R.R., Bendifallah, I., Grimm, C., Lafirdeen, A.S.M., Domínguez, S., Chan, C.Y., Lu, X., Forget, B.C., St-Pierre, F., Papagiakoumou, E., et al. (2024). Scanless two-photon voltage imaging. Nat. Commun. *15*, 5095. https://doi.org/10.1038/s41467-024-49192-2.

27. Wang, Z., Sims, R.R., Xiao, S., Zhao, R., Benshlomo, O., Zang, Z., Wu, J., Emiliani, V., and Gao, L. (2026). High-speed optical microscopy for neural voltage imaging: Methods, trade-offs, and opportunities. Preprint at arXiv. https://doi.org/10.48550/arXiv.2512.15587.

28. Silva, R., Bartalis-Szélyes, H., Brinks, D., and Gao, Z. (2025). Robustness and fidelity of voltage imaging analysis pipelines. Preprint at bioRxiv. https://doi.org/10.1101/2025.09.26.678573.

29. Huang, Y.-C., Chen, H.-C., Lin, Y.-T., Lin, S.-T., Zheng, Q., Abdelfattah, A.S., Lavis, L.D., Schreiter, E.R., Lin, B.-J., and Chen, T.-W. (2024). Dynamic assemblies of parvalbumin interneurons in brain oscillations. Neuron *112*, 2600–2613.e5. https://doi.org/10.1016/j.neuron.2024.05.015.

30. Taxidis, J., Madruga, B., Safaryan, K., Dorian, C.C., Melin, M.D., Day, Z., Lin, M.Z., and Golshani, P. (2025). Voltage imaging reveals hippocampal inhibitory dynamics shaping pyramidal memory-encoding sequences. Nat. Neurosci. *28*, 1946–1958. https://doi.org/10.1038/s41593-025-02016-y.

31. Brown, S.T., Holla, M.R., Land, M.A., Yang, S., McDonald, A.J., St-Pierre, F., and Raman, I.M. (2025). High-speed voltage imaging of action potentials in molecular layer interneurons reveals sensory-driven synchrony that augments movement. Cell Rep. *44*, 116148. https://doi.org/10.1016/j.celrep.2025.116148.

32. Park, J., Werley, C.A., Venkatachalam, V., Kralj, J.M., Dib-Hajj, S.D., Waxman, S.G., and Cohen, A.E. (2013). Screening fluorescent voltage indicators with spontaneously spiking HEK cells. PLoS One *8*, e85221. https://doi.org/10.1371/journal.pone.0085221.

33. Zhang, H., Reichert, E., and Cohen, A.E. (2016). Optical electrophysiology for probing function and pharmacology of voltage-gated ion channels. eLife *5*, e15202. https://doi.org/10.7554/eLife.15202.

34. Saminathan, A., Devany, J., Veetil, A.T., Suresh, B., Pillai, K.S., Schwake, M., and Krishnan, Y. (2021). A DNA-based voltmeter for organelles. Nat. Nanotechnol. *16*, 96–103. https://doi.org/10.1038/s41565-020-00784-1.

35. Gong, Y., Huang, C., Li, J.Z., Grewe, B.F., Zhang, Y., Eismann, S., and Schnitzer, M.J. (2015). High-speed recording of neural spikes in awake mice and flies with a fluorescent voltage sensor. Science *350*, 1361–1366. https://doi.org/10.1126/science.aab0810.

36. Piatkevich, K.D., Bensussen, S., Tseng, H.A., Shroff, S.N., Lopez-Huerta, V.G., Park, D., Jung, E.E., Shemesh, O.A., Straub, C., Gritton, H.J., et al. (2019). Population imaging of neural activity in awake behaving mice. Nature *574*, 413–417. https://doi.org/10.1038/s41586-019-1641-1.

37. Abdelfattah, A.S., Kawashima, T., Singh, A., Novak, O., Liu, H., Shuai, Y., Huang, Y.-C., Campagnola, L., Seeman, S.C., Yu, J., et al. (2019). Bright and photostable chemigenetic indicators for extended in vivo voltage imaging. Science *365*, 699–704. https://doi.org/10.1126/science.aav6416.

38. Williams, L.A., Ryan, S.J., Joshi, V., Lewarch, C., Elder, A., McManus, O., Godard, P., Sridhar, S., Jacques, J., Grooms, J., et al. (2024). Discovery of novel compounds and target mechanisms using a high throughput, multiparametric phenotypic screen in a human neuronal model of Tuberous Sclerosis. Preprint at bioRxiv. https://doi.org/10.1101/2024.02.22.581652.

39. Zhang, H., Moyer, B.D., Yu, V., McGivern, J.G., Jarosh, M., Werley, C.A., Hecht, V.C., Babcock, R.J., Dong, K., Dempsey, G.T., et al. (2020). Correlation of Optical and Automated Patch Clamp Electrophysiology for Identification of NaV1.7 Inhibitors. SLAS Discov. *25*, 434–446. https://doi.org/10.1177/2472555220914532.

40. Kiskinis, E., Kralj, J.M., Zou, P., Weinstein, E.N., Zhang, H., Tsioras, K., Wiskow, O., Ortega, J.A., Eggan, K., and Cohen, A.E. (2018). All-Optical Electrophysiology for High-Throughput Functional Characterization of a Human iPSC-Derived Motor Neuron Model of ALS. Stem Cell Rep. *10*, 1991–2004. https://doi.org/10.1016/j.stemcr.2018.04.020.

41. Werley, C.A., Brookings, T., Upadhyay, H., Williams, L.A., McManus, O.B., and Dempsey, G.T. (2017). All-Optical Electrophysiology for Disease Modeling and Pharmacological Characterization of Neurons. Curr. Protoc. Pharmacol. *78*, 11.20.1–11.20.24.

42. Park, P., Wong-Campos, J.D., Itkis, D.G., Lee, B.H., Qi, Y., Davis, H.C., Antin, B., Pasarkar, A., Grimm, J.B., Plutkis, S.E., et al. (2025). Dendritic excitations govern back-propagation via a spike-rate accelerometer. Nat. Commun. *16*, 1333. https://doi.org/10.1038/s41467-025-55819-9.

43. Haziza, S., Chrapkiewicz, R., Zhang, Y., Kruzhilin, V., Li, J., Li, J., Delamare, G., Swanson, R., Buzsáki, G., Kannan, M., et al. (2025). Imaging high-frequency voltage dynamics in multiple neuron classes of behaving mammals. Cell *188*, 4401–4423.e31. https://doi.org/10.1016/j.cell.2025.06.028.

44. Lowet, E., Sheehan, D.J., Chialva, U., De Oliveira Pena, R., Mount, R.A., Xiao, S., Zhou, S.L., Tseng, H.A., Gritton, H., Shroff, S., et al. (2023). Theta and gamma rhythmic coding through two spike output modes in the hippocampus during spatial navigation. Cell Rep. *42*, 112906. https://doi.org/10.1016/j.celrep.2023.112906.

45. Liu, P.W., Zhang, H., Werley, C.A., Pichler, M., Ryan, S.J., Lewarch, C.L., Jacques, J., Grooms, J., Ferrante, J., Li, G., et al. (2024). A phenotypic screening platform for chronic pain therapeutics using all-optical electrophysiology. Pain *165*, 922–940. https://doi.org/10.1097/j.pain.0000000000003090.

46. Csillag, V., Bizzozzero, M.H., Noble, J.C., Reinius, B., and Fuzik, J. (2023). Voltage-Seq: all-optical postsynaptic connectome-guided single-cell transcriptomics. Nat. Methods *20*, 1409–1416. https://doi.org/10.1038/s41592-023-01965-1.

47. Layous, R., Tamás, B., Mike, A., Sipos, E., Arszovszki, A., Brunner, J., Szatai, Á., Yaseen, F., Andrási, T., and Szabadics, J. (2025). Optical recordings of unitary synaptic connections reveal high and random local connectivity between CA3 pyramidal cells. J. Neurosci. *45*, e0102252025. https://doi.org/10.1523/JNEUROSCI.0102-25.2025.

48. Moya, M.V., Cunningham, W.J., Vincent, J.P., Wang, T., and Economo, M.N. (2025). A scalable, all-optical method for mapping synaptic connectivity with cell-type specificity. Preprint at bioRxiv. https://doi.org/10.1101/2025.06.25.661552.

49. Carolan, J., Land, M.A., Lu, X., Beau, M., Kostadinov, D., St-Pierre, F., Clark, B.A., and Häusser, M. (2025). All-optical voltage interrogation for probing synaptic plasticity in vivo. Nat. Commun. *16*, 8834. https://doi.org/10.1038/s41467-025-63867-4.

50. Fan, L.Z., Nehme, R., Adam, Y., Jung, E.S., Wu, H., Eggan, K., Arnold, D.B., and Cohen, A.E. (2018). All-optical synaptic electrophysiology probes mechanism of ketamine-induced disinhibition. Nat. Methods *15*, 823–831. https://doi.org/10.1038/s41592-018-0142-8.

51. Fan, L.Z., Kim, D.K., Jennings, J.H., Tian, H., Wang, P.Y., Ramakrishnan, C., Randles, S., Sun, Y., Thadhani, E., Kim, Y.S., et al. (2023). All-optical physiology resolves a synaptic basis for behavioral timescale plasticity. Cell *186*, 543–559.e19. https://doi.org/10.1016/j.cell.2022.12.035.

52. Gonzalez, K.C., Negrean, A., Liao, Z., Terada, S., Zhang, G., Lee, S., Ócsai, K., Rózsa, B.J., Lin, M.Z., Polleux, F., et al. (2025). Synaptic basis of feature selectivity in hippocampal neurons. Nature *637*, 1152–1160. https://doi.org/10.1038/s41586-024-08325-9.

53. Gonzalez, K.C., Terada, S., Noguchi, A., Zakka, G.N., O'Toole, C., Bilbao, G., Reynolds, L., Jász, A., Kertész, B., Szadai, Z., et al. (2026). Movement-stabilized three-dimensional optical recordings of membrane potential changes and calcium dynamics in hippocampal CA1 dendrites. Neuron *114*, 1818–1832.e9. https://doi.org/10.1016/j.neuron.2026.01.004.

54. Hoppa, M.B., Gouzer, G., Armbruster, M., and Ryan, T.A. (2014). Control and plasticity of the presynaptic action potential waveform at small CNS nerve terminals. Neuron *84*, 778–789. https://doi.org/10.1016/j.neuron.2014.09.038.

55. Lou, S., Adam, Y., Weinstein, E.N., Williams, E., Williams, K., Parot, V., Kavokine, N., Liberles, S., Madisen, L., Zeng, H., et al. (2016). Genetically targeted all-optical electrophysiology with a transgenic Cre-dependent Optopatch mouse. J. Neurosci. *36*, 11059–11073. https://doi.org/10.1523/JNEUROSCI.1582-16.2016.

56. Wong-Campos, J.D., Park, P., Lee, B.H., Davis, H.C., Qi, Y., Tian, H., Itkis, D.G., Kim, D., Grimm, J.B., Plutkis, S.E., et al. (2026). Voltage dynamics of cortical dendrites in vivo. Nat. Neurosci. *29*, 1885–1893. https://doi.org/10.1038/s41593-026-02339-4.

57. Liao, Z., Gonzalez, K.C., Li, D.M., Yang, C.M., Holder, D., McClain, N.E., Zhang, G., Evans, S.W., Chavarha, M., Simko, J., et al. (2024). Functional architecture of intracellular oscillations in hippocampal dendrites. Nat. Commun. *15*, 6295. https://doi.org/10.1038/s41467-024-50546-z.

58. Azimi Hashemi, N., Bergs, A.C.F., Schüler, C., Scheiwe, A.R., Steuer Costa, W., Bach, M., Liewald, J.F., and Gottschalk, A. (2019). Rhodopsin-based voltage imaging tools for use in muscles and neurons of Caenorhabditis elegans. Proc. Natl. Acad. Sci. USA *116*, 17051–17060. https://doi.org/10.1073/pnas.1902443116.

59. Huang, C., Luo, J., Woo, S.J., Roitman, L.A., Li, J., Pieribone, V.A., Kannan, M., Vasan, G., and Schnitzer, M.J. (2024). Dopamine-mediated interactions between short- and long-term memory dynamics. Nature *634*, 1141–1149. https://doi.org/10.1038/s41586-024-07819-w.

60. Kawashima, T., Wei, Z., Haruvi, R., Shainer, I., Narayan, S., Baier, H., and Ahrens, M.B. (2025). Voltage imaging reveals circuit computations in the raphe underlying serotonin-mediated motor vigor learning. Neuron *113*, 2692–2707.e8. https://doi.org/10.1016/j.neuron.2025.05.017.

61. Böhm, U.L., Kimura, Y., Kawashima, T., Ahrens, M.B., Higashijima, S.I., Engert, F., and Cohen, A.E. (2022). Voltage imaging identifies spinal circuits that modulate locomotor adaptation in zebrafish. Neuron *110*, 1211–1222.e4. https://doi.org/10.1016/j.neuron.2022.01.001.

62. Huys, Q.J.M., Ahrens, M.B., and Paninski, L. (2006). Efficient estimation of detailed single-neuron models. J. Neurophysiol. *96*, 872–890. https://doi.org/10.1152/jn.00079.2006.

63. Fink, J.J., Delaney-Busch, N., Dawes, R., Nanou, E., Folts, C., Harikrishnan, K., Hempel, C., Upadhyay, H., Nguyen, T., Shroff, H., et al. (2024). Deep functional measurements of Fragile X syndrome human neurons reveal multiparametric electrophysiological disease phenotype. Commun. Biol. *7*, 1447. https://doi.org/10.1038/s42003-024-07120-6.

64. Yang, Q., Baror-Sebban, S., Kipper, R., London, M., and Adam, Y. (2025). All-optical electrophysiology reveals behavior-dependent dynamics of excitation and inhibition in the hippocampus. Neuron *114*, 1635–1650.e7. https://doi.org/10.1016/j.neuron.2025.12.040.

65. Hochbaum, D.R., Zhao, Y., Farhi, S.L., Klapoetke, N., Werley, C.A., Kapoor, V., Zou, P., Kralj, J.M., Maclaurin, D., Smedemark-Margulies, N., et al. (2014). All-optical electrophysiology in mammalian neurons using engineered microbial rhodopsins. Nat. Methods *11*, 825–833. https://doi.org/10.1038/nmeth.3000.

66. Fan, L.Z., Kheifets, S., Böhm, U.L., Wu, H., Piatkevich, K.D., Xie, M.E., Parot, V., Ha, Y., Evans, K.E., Boyden, E.S., et al. (2020). All-Optical Electrophysiology Reveals the Role of Lateral Inhibition in Sensory Processing in Cortical Layer 1. Cell *180*, 521–535.e18. https://doi.org/10.1016/j.cell.2020.01.001.

67. Xiao, S., Lowet, E., Gritton, H.J., Fabris, P., Wang, Y., Sherman, J., Mount, R.A., Tseng, H.-A., Man, H.-Y., Straub, C., et al. (2021). Large-scale voltage imaging in behaving mice using targeted illumination. iScience *24*, 103263. https://doi.org/10.1016/j.isci.2021.103263.

68. Kannan, M., Vasan, G., Haziza, S., Huang, C., Chrapkiewicz, R., Luo, J., Cardin, J.A., Schnitzer, M.J., and Pieribone, V.A. (2022). Dual-polarity voltage imaging of the concurrent dynamics of multiple neuron types. Science *378*, eabm8797. https://doi.org/10.1126/science.abm8797.

69. Armbruster, M., Naskar, S., Garcia, J.P., Sommer, M., Kim, E., Adam, Y., Haydon, P.G., Boyden, E.S., Cohen, A.E., and Dulla, C.G. (2022). Neuronal activity drives pathway-specific depolarization of peripheral astrocyte processes. Nat. Neurosci. *25*, 607–616. https://doi.org/10.1038/s41593-022-01049-x.

70. Wilt, B.A., Fitzgerald, J.E., and Schnitzer, M.J. (2013). Photon Shot Noise Limits on Optical Detection of Neuronal Spikes and Estimation of Spike Timing. Biophys. J. *104*, 51–62. https://doi.org/10.1016/j.bpj.2012.07.058.

71. Brooks III, F.P., Davis, H.C., Wong-Campos, J.D., and Cohen, A.E. (2024). Optical constraints on two-photon voltage imaging. Neurophotonics *11*, 035007. https://doi.org/10.1117/1.NPh.11.3.035007.

72. Hao, Y.A., Jayne, L.L., Lee, S., Dittrich, M.N., Zhang, M., Haziza, S., Bendifallah, I., Sims, R.R., Bouazza-Arostegui, B., White, A.D., et al. (2026). Ultrasensitive voltage imaging reveals distinct electrical microdomains in neurons. Preprint at bioRxiv. https://doi.org/10.64898/2026.05.27.728040.

73. Podgorski, K., and Ranganathan, G. (2016). Brain heating induced by near-infrared lasers during multiphoton microscopy. J. Neurophysiol. *116*, 1012–1023. https://doi.org/10.1152/jn.00275.2016.

74. Wäldchen, S., Lehmann, J., Klein, T., van de Linde, S., and Sauer, M. (2015). Light-induced cell damage in live-cell super-resolution microscopy. Sci. Rep. *5*, 15348. https://doi.org/10.1038/srep15348.

75. Reinert, K.C., Dunbar, R.L., Gao, W., Chen, G., and Ebner, T.J. (2004). Flavoprotein Autofluorescence Imaging of Neuronal Activation in the Cerebellar Cortex In Vivo. J. Neurophysiol. *92*, 199–211. https://doi.org/10.1152/jn.01275.2003.

76. Binns, T.C., Ayala, A.X., Grimm, J.B., Tkachuk, A.N., Castillon, G.A., Phan, S., Zhang, L., Brown, T.A., Liu, Z., Adams, S.R., et al. (2020). Rational Design of Bioavailable Photosensitizers for Manipulation and Imaging of Biological Systems. Cell Chem. Biol. *27*, 1063–1072.e7. https://doi.org/10.1016/j.chembiol.2020.07.001.

77. Abdelfattah, A.S., Zheng, J., Singh, A., Huang, Y.-C., Reep, D., Tsegaye, G., Tsang, A., Arthur, B.J., Rehorova, M., Olson, C.V.L., et al. (2023). Sensitivity optimization of a rhodopsin-based fluorescent voltage indicator. Neuron *111*, 1547–1563.e9. https://doi.org/10.1016/j.neuron.2023.03.009.

78. Cao, C., Zhu, R., Zhou, S., Zhao, Z., Lin, C., Liu, S., Peng, L., Subach, F.V., Piatkevich, K.D., and Zou, P. (2025). A photostable genetically encoded voltage indicator for imaging neural activities in tissue and live animals. Preprint at bioRxiv. https://doi.org/10.1101/2025.05.29.656768.

79. Zhang, H., Zhou, S., Kuzmicheva, T.P., Subach, O.M., Grimm, C., Eom, M., Baror-Sebban, S., Adam, Y., Yoon, Y.-G., Emilliani, V., et al. (2025). Bright and Photostable Voltage Sensors Derived from mBaoJin. Preprint at bioRxiv. https://doi.org/10.1101/2025.05.30.657123.

80. Abdelfattah, A.S., Valenti, R., Zheng, J., Wong, A., GENIE Project Team, Podgorski, K., Koyama, M., Kim, D.S., and Schreiter, E.R. (2020). A general approach to engineer positive-going eFRET voltage indicators. Nat. Commun. *11*, 3444. https://doi.org/10.1038/s41467-020-17322-1.

81. Jacques, S.L. (2013). Optical properties of biological tissues: a review. Phys. Med. Biol. *58*, R37–R61. https://doi.org/10.1088/0031-9155/58/11/R37.

82. Yaroslavsky, A.N., Schulze, P.C., Yaroslavsky, I.V., Schober, R., Ulrich, F., and Schwarzmaier, H.J. (2002). Optical properties of selected native and coagulated human brain tissues in vitro in the visible and near infrared spectral range. Phys. Med. Biol. *47*, 2059–2073. https://doi.org/10.1088/0031-9155/47/12/305.

83. Venkatachalam, V., and Cohen, A.E. (2014). Imaging GFP-based reporters in neurons with multiwavelength optogenetic control. Biophys. J. *107*, 1554–1563. https://doi.org/10.1016/j.bpj.2014.08.020.

84. Farhi, S.L., Parot, V.J., Grama, A., Yamagata, M., Abdelfattah, A.S., Adam, Y., Lou, S., Kim, J.J., Campbell, R.E., Cox, D.D., et al. (2019). Wide-Area All-Optical Neurophysiology in Acute Brain Slices. J. Neurosci. *39*, 4889–4908. https://doi.org/10.1523/JNEUROSCI.0168-19.2019.

85. Hou, J.H., Kralj, J.M., Douglass, A.D., Engert, F., and Cohen, A.E. (2014). Simultaneous mapping of membrane voltage and calcium in zebrafish heart in vivo reveals chamber-specific developmental transitions in ionic currents. Front. Physiol. *5*, 344. https://doi.org/10.3389/fphys.2014.00344.

86. Aggarwal, A., Liu, R., Chen, Y., Ralowicz, A.J., Bergerson, S.J., Tomaska, F., Mohar, B., Hanson, T.L., Hasseman, J.P., Reep, D., et al. (2023). Glutamate indicators with improved activation kinetics and localization for imaging synaptic transmission. Nat. Methods *20*, 925–934. https://doi.org/10.1038/s41592-023-01863-6.

87. Aggarwal, A., Negrean, A., Chen, Y., Iyer, R., Reep, D., Liu, A., Palutla, A., Xie, M.E., MacLennan, B.J., Hagihara, K.M., et al. (2025). Glutamate indicators with increased sensitivity and tailored deactivation rates. Nat. Methods *23*, 417–425. https://doi.org/10.1038/s41592-025-02965-z.

88. McDonald, A.J., Land, M.A., Yang, S., Hakam, N., Villette, V., Zhu, J., Galdamez, M., de La Puebla, M.F., Lu, X., Foran, G., et al. (2026). A versatile, positive-going voltage indicator that enables accessible two-photon recordings in vivo. Preprint at bioRxiv. https://doi.org/10.64898/2026.04.07.717088.

89. Sakamoto, M., and Yokoyama, T. (2025). Probing neuronal activity with genetically encoded calcium and voltage fluorescent indicators. Neurosci. Res. *215*, 56–63. https://doi.org/10.1016/j.neures.2024.06.004.

90. Monakhov, M.V., Matlashov, M.E., Colavita, M., Song, C., Shcherbakova, D.M., Antic, S.D., Verkhusha, V.V., and Knöpfel, T. (2020). Screening and Cellular Characterization of Genetically Encoded Voltage Indicators Based on Near-Infrared Fluorescent Proteins. ACS Chem. Neurosci. *11*, 3523–3531. https://doi.org/10.1021/acschemneuro.0c00046.

91. Czuchnowski, J., and Mertz, J. (2026). Implications of temporal sampling in voltage imaging microscopy. Preprint at arXiv. https://doi.org/10.48550/arXiv.2601.20236.

92. St-Pierre, F., Marshall, J.D., Yang, Y., Gong, Y., Schnitzer, M.J., and Lin, M.Z. (2014). High-fidelity optical reporting of neuronal electrical activity with an ultrafast fluorescent voltage sensor. Nat. Neurosci. *17*, 884–889. https://doi.org/10.1038/nn.3709.

93. Lee, S., Zhang, G., Hao, Y.A., Roth, R.H., Sun, Y., Dong, C., Zhu, J., Gomez, L.C., Natan, R.G., Jiang, D., et al. (2026). Improving positively tuned voltage indicators for faster kinetics and higher contrast. Preprint at bioRxiv. https://doi.org/10.1101/2024.06.21.599617.

94. Kralj, J.M., Hochbaum, D.R., Douglass, A.D., and Cohen, A.E. (2011). Electrical spiking in Escherichia coli probed with a fluorescent voltage-indicating protein. Science *333*, 345–348. https://doi.org/10.1126/science.1204763.

95. Kralj, J.M., Douglass, A.D., Hochbaum, D.R., Maclaurin, D., and Cohen, A.E. (2011). Optical recording of action potentials in mammalian neurons using a microbial rhodopsin. Nat. Methods *9*, 90–95. https://doi.org/10.1038/nmeth.1782.

96. Piatkevich, K.D., Jung, E.E., Straub, C., Linghu, C., Park, D., Suk, H.-J., Hochbaum, D.R., Goodwin, D., Pnevmatikakis, E., Pak, N., et al. (2018). A robotic multidimensional directed evolution approach applied to fluorescent voltage reporters. Nat. Chem. Biol. *14*, 352–360. https://doi.org/10.1038/s41589-018-0004-9.

97. Tian, H., Davis, H.C., Wong-Campos, J.D., Park, P., Fan, L.Z., Gmeiner, B., Begum, S., Werley, C.A., Borja, G.B., Upadhyay, H., et al. (2023). Video-based pooled screening yields improved far-red genetically encoded voltage indicators. Nat. Methods *20*, 1082–1094. https://doi.org/10.1038/s41592-022-01743-5.

98. Maclaurin, D., Venkatachalam, V., Lee, H., and Cohen, A.E. (2013). Mechanism of voltage-sensitive fluorescence in a microbial rhodopsin. Proc. Natl. Acad. Sci. USA *110*, 5939–5944. https://doi.org/10.1073/pnas.1215595110.

99. Zou, P., Zhao, Y., Douglass, A.D., Hochbaum, D.R., Brinks, D., Werley, C.A., Harrison, D.J., Campbell, R.E., and Cohen, A.E. (2014). Bright and fast multicoloured voltage reporters via electrochromic FRET. Nat. Commun. *5*, e4625. https://doi.org/10.1038/ncomms5625.

100. Gong, Y., Wagner, M.J., Li, J.Z., and Schnitzer, M.J. (2014). Imaging neural spiking in brain tissue using FRET-opsin protein voltage sensors. Nat. Commun. *5*, 3674. https://doi.org/10.1038/ncomms4674.

101. Kannan, M., Vasan, G., Huang, C., Haziza, S., Li, J.Z., Inan, H., Schnitzer, M.J., and Pieribone, V.A. (2018). Fast, in vivo voltage imaging using a red fluorescent indicator. Nat. Methods *15*, 1108–1116. https://doi.org/10.1038/s41592-018-0188-7.

102. Wong-Campos, J.D., Park, P., Lee, B.H., Davis, H.C., Qi, Y., Tian, H., Itkis, D.G., Kim, D., Grimm, J.B., Plutkis, S.E., et al. (2026). Voltage dynamics of cortical dendrites in vivo. Nat. Neurosci. *29*, 1885–1893. https://doi.org/10.1038/s41593-026-02339-4.

103. Bai, L., Cong, L., Shi, Z., Zhao, Y., Zhang, Y., Lu, B., Zhang, J., Xiong, Z.-Q., Xu, N., Mu, Y., et al. (2024). Volumetric voltage imaging of neuronal populations in the mouse brain by confocal light-field microscopy. Nat. Methods *21*, 2160–2170. https://doi.org/10.1038/s41592-024-02458-5.

104. Brinks, D., Klein, A.J., and Cohen, A.E. (2015). Two-Photon Lifetime Imaging of Voltage Indicating Proteins as a Probe of Absolute Membrane Voltage. Biophys. J. *109*, 914–921. https://doi.org/10.1016/j.bpj.2015.07.038.

105. Villette, V., Yang, S., Valenti, R., Macklin, J.J., Bradley, J., Mathieu, B., Lombardini, A., Podgorski, K., Dieudonné, S., Schreiter, E.R., et al. (2024). A novel rhodopsin-based voltage indicator for simultaneous two-photon optical recording with GCaMP in vivo. Preprint at bioRxiv. https://doi.org/10.1101/2024.11.15.623698.

106. Chien, M.-P., Brinks, D., Testa-Silva, G., Tian, H., Phil Brooks, F., Adam, Y., Bloxham, B., Gmeiner, B., Kheifets, S., and Cohen, A.E. (2021). Photoactivated voltage imaging in tissue with an Archaerhodopsin-derived reporter. Sci. Adv. *7*, eabe3216. https://doi.org/10.1126/sciadv.abe3216.

107. Brooks, F.P., Gong, D., Davis, H.C., Park, P., Qi, Y., and Cohen, A.E. (2025). Photophysics-informed two-photon voltage imaging using FRET-opsin voltage indicators. Sci. Adv. *11*, eadp5763. https://doi.org/10.1126/sciadv.adp5763.

108. Huang, C., Maxey, J.R., Sinha, S., Savall, J., Gong, Y., and Schnitzer, M.J. (2018). Long-term optical brain imaging in live adult fruit flies. Nat. Commun. *9*, 872. https://doi.org/10.1038/s41467-018-02873-1.

109. Kubota, Y., Karube, F., Nomura, M., Gulledge, A.T., Mochizuki, A., Schertel, A., and Kawaguchi, Y. (2011). Conserved properties of dendritic trees in four cortical interneuron subtypes. Sci. Rep. *1*, 89. https://doi.org/10.1038/srep00089.

110. Birinyi, A., Antal, M., Wolf, E., and Székely, G. (1992). The extent of the dendritic tree and the number of synapses in the frog motoneuron. Eur. J. Neurosci. *4*, 1003–1012. https://doi.org/10.1111/j.1460-9568.1992.tb00127.x.

111. Lim, S.T., Antonucci, D.E., Scannevin, R.H., and Trimmer, J.S. (2000). A novel targeting signal for proximal clustering of the Kv2.1 K+ channel in hippocampal neurons. Neuron *25*, 385–397. https://doi.org/10.1016/S0896-6273(00)80902-2.

112. Wu, C., Ivanova, E., Zhang, Y., and Pan, Z.-H. (2013). rAAV-mediated subcellular targeting of optogenetic tools in retinal ganglion cells in vivo. PLoS One *8*, e66332. https://doi.org/10.1371/journal.pone.0066332.

113. Chettih, S.N., and Harvey, C.D. (2019). Single-neuron perturbations reveal feature-specific competition in V1. Nature *567*, 334–340. https://doi.org/10.1038/s41586-019-0997-6.

114. Shepard, B.D., Natarajan, N., Protzko, R.J., Acres, O.W., and Pluznick, J.L. (2013). A cleavable N-terminal signal peptide promotes widespread olfactory receptor surface expression in HEK293T cells. PLoS One *8*, e68758. https://doi.org/10.1371/journal.pone.0068758.

115. Rühl, P., Nair, A.G., Gawande, N., Dehiwalage, S.N.C.W., Münster, L., Schönherr, R., and Heinemann, S.H. (2024). An Ultrasensitive Genetically Encoded Voltage Indicator Uncovers the Electrical Activity of Non-Excitable Cells. Adv. Sci. (Weinh) *11*, e2307938. https://doi.org/10.1002/advs.202307938.

116. Nair, A.G., Rodewald, M., Bae, H., Rühl, P., Popp, J., Schmitt, M., Meyer-Zedler, T., and Heinemann, S.H. (2025). Absolute Membrane Potential Recording with ASAP-Type Genetically Encoded Voltage Indicators Using Fluorescence Lifetime Imaging. ACS Chem. Neurosci. *16*, 4636–4646. https://doi.org/10.1101/2025.08.08.669310.

117. Hou, J.H., Venkatachalam, V., and Cohen, A.E. (2014). Temporal dynamics of microbial rhodopsin fluorescence reports absolute membrane voltage. Biophys. J. *106*, 639–648. https://doi.org/10.1016/j.bpj.2013.11.4493.

118. Venkatachalam, V., Brinks, D., Maclaurin, D., Hochbaum, D., Kralj, J., and Cohen, A.E. (2014). Flash memory: photochemical imprinting of neuronal action potentials onto a microbial rhodopsin. J. Am. Chem. Soc. *136*, 2529–2537. https://doi.org/10.1021/ja411338t.

119. Sepehri Rad, M., Cohen, L.B., Braubach, O., and Baker, B.J. (2018). Monitoring voltage fluctuations of intracellular membranes. Sci. Rep. *8*, 6911. https://doi.org/10.1038/s41598-018-25083-7.

120. Ronzitti, E., Ventalon, C., Canepari, M., Forget, B.C., Papagiakoumou, E., and Emiliani, V. (2017). Recent advances in patterned photostimulation for optogenetics. J. Opt. *19*, 113001. https://doi.org/10.1088/2040-8986/aa8299.

121. Emiliani, V., Cohen, A.E., Deisseroth, K., and Häusser, M. (2015). All-optical interrogation of neural circuits. J. Neurosci. *35*, 13917–13926. https://doi.org/10.1523/JNEUROSCI.2916-15.2015.

122. Hannebelle, M.T.M., Raeth, E., Leitao, S.M., Lukeš, T., Pospíšil, J., Toniolo, C., Venzin, O.F., Chrisnandy, A., Swain, P.P., Ronceray, N., et al. (2024). Open-source microscope add-on for structured illumination microscopy. Nat. Commun. *15*, 1550. https://doi.org/10.1038/s41467-024-45567-7.

123. Xiao, S., Cunningham, W.J., Kondabolu, K., Lowet, E., Moya, M.V., Mount, R.A., Ravasio, C., Bortz, E., Shaw, D., Economo, M.N., et al. (2024). Large-scale deep tissue voltage imaging with targeted-illumination confocal microscopy. Nat. Methods *21*, 1094–1102. https://doi.org/10.1038/s41592-024-02275-w.

124. Wu, X., Lee, B.H., Park, P., Wong-Campos, J.D., Xu, J., Plutkis, S.E., Lavis, L.D., and Cohen, A.E. (2026). A dendrite-resolved, *in vivo* transfer function from spike patterns to dendritic Ca^{2+}. Preprint at bioRxiv. https://doi.org/10.64898/2026.01.18.700189.

125. Wang, Z., Zhang, J., Symvoulidis, P., Guo, W., Deng, D., Amsterdam, A., Zhang, L., Honda, T., Roche, S., Wilson, M.A., and Boyden, E.S. (2026). Voltage imaging of neurons distributed across entire brains of larval zebrafish. Nat. Methods Published online. August 14, 2026. https://doi.org/10.1038/s41592-026-03179-7.

126. Böhm, U.L., and Judkewitz, B. (2024). Fast and light-efficient remote focusing for volumetric voltage imaging. Nat. Commun. *15*, 9555. https://doi.org/10.1038/s41467-024-53685-5.

127. Dunsby, C. (2008). Optically sectioned imaging by oblique plane microscopy. Opt. Express *16*, 20306–20316. https://doi.org/10.1364/OE.16.020306.

128. Kim, S., Yoon, J., Ko, G., Kang, I., Tian, H., Fan, L.Z., Li, Y., Xiao, G., Zhang, Q., Cohen, A.E., et al. (2025). Optical segmentation-based

compressed readout of neuronal voltage dynamics. Nat. Commun. *16*, 7194. https://doi.org/10.1038/s41467-025-62663-4.

129. Quicke, P., Howe, C.L., Song, P., Jadan, H.V., Song, C., Knöpfel, T., Neil, M., Dragotti, P.L., Schultz, S.R., and Foust, A.J. (2020). Subcellular resolution three-dimensional light-field imaging with genetically encoded voltage indicators. Neurophotonics *7*, 035006. https://doi.org/10.1117/1.NPh.7.3.035006.

130. Itkis, D.G., Brooks, F.P., Davis, H.C., Hotter, R., Wong-Campos, J.D., Qi, Y., Jia, B.Z., Howell, M., Xiong, M., Hayward, R.F., et al. (2025). Luminos: open-source software for bidirectional microscopy. Preprint at bioRxiv. https://doi.org/10.1101/2025.02.22.639658.

131. Salomé, R., Kremer, Y., Dieudonné, S., Léger, J.F., Krichevsky, O., Wyart, C., Chatenay, D., and Bourdieu, L. (2006). Ultrafast random-access scanning in two-photon microscopy using acousto-optic deflectors. J. Neurosci. Methods *154*, 161–174. https://doi.org/10.1016/j.jneumeth.2005.12.010.

132. Villette, V., Chavarha, M., Dimov, I.K., Bradley, J., Pradhan, L., Mathieu, B., Evans, S.W., Chamberland, S., Shi, D., Yang, R., et al. (2019). Ultrafast Two-Photon Imaging of a High-Gain Voltage Indicator in Awake Behaving Mice. Cell *179*, 1590–1608.e23. https://doi.org/10.1016/j.cell.2019.11.004.

133. Katona, G., Szalay, G., Maák, P., Kaszás, A., Veress, M., Hillier, D., Chiovini, B., Vizi, E.S., Roska, B., and Rózsa, B. (2012). Fast two-photon in vivo imaging with three-dimensional random-access scanning in large tissue volumes. Nat. Methods *9*, 201–208. https://doi.org/10.1038/nmeth.1851.

134. Nadella, K.M.N.S., Roš, H., Baragli, C., Griffiths, V.A., Konstantinou, G., Koimtzis, T., Evans, G.J., Kirkby, P.A., and Silver, R.A. (2016). Random-access scanning microscopy for 3D imaging in awake behaving animals. Nat. Methods *13*, 1001–1004. https://doi.org/10.1038/nmeth.4033.

135. Zhong, J., Natan, R.G., Zhang, Q., Wong, J.S.J., Miehl, C., Bose, K., Lu, X., St-Pierre, F., Guo, S., Doiron, B., et al. (2025). FACED 2.0 enables large-scale voltage and calcium imaging in vivo. Nat. Methods *23*, 1611–1621. https://doi.org/10.1038/s41592-025-02925-7.

136. Zhang, M., Liu, S., Zhao, Y., Zhu, Y., Gu, X., Kong, C., Hu, J., Yu, H., Wu, J., Xu, F., et al. (2026). Kilohertz-rate two-photon voltage imaging of population dynamics in vivo. Preprint at bioRxiv. https://doi.org/10.64898/2025.12.29.696942.

137. Demas, J., Manley, J., Tejera, F., Barber, K., Kim, H., Traub, F.M., Chen, B., and Vaziri, A. (2021). High-speed, cortex-wide volumetric recording of neuroactivity at cellular resolution using light beads microscopy. Nat. Methods *18*, 1103–1111. https://doi.org/10.1038/s41592-021-01239-8.

138. Zhang, Z., Liu, S.-J., Mattison, B., Muir, J., Spurr, N., Kim, C.K., and Yang, W. (2025). High-speed neural imaging with multiplexed miniaturized two-photon microscopy. Cell Rep. Methods *5*, 101221. https://doi.org/10.1016/j.crmeth.2025.101221.

139. Zhao, S., Hebert, E., Gruzdeva, A., Mahishi, D., Takahashi, H., Lee, S., Hao, Y.A., Lin, M.Z., Yapici, N., and Xu, C. (2024). Deep two-photon voltage imaging with adaptive excitation. Preprint at Research Square. https://doi.org/10.21203/rs.3.rs-5434919/v1.

140. Buchanan, E.K., Kinsella, I., Zhou, D., Zhu, R., Zhou, P., Gerhard, F., Ferrante, J., Ma, Y., Kim, S., and Shaik, M. (2018). Penalized matrix decomposition for denoising, compression, and improved demixing of functional imaging data. Preprint at bioRxiv.

141. Pasarkar, A., Kinsella, I., Zhou, P., Wu, M., Pan, D., Fan, J.L., Wang, Z., Abdeladim, L., Peterka, D.S., Adesnik, H., et al. (2023). maskNMF: A denoise-sparsen-detect approach for extracting neural signals from dense imaging data. Preprint at bioRxiv. https://doi.org/10.1101/2023.09.14.557777.

142. Pnevmatikakis, E.A., and Giovannucci, A. (2017). NoRMCorre: An online algorithm for piecewise rigid motion correction of calcium imaging data. J. Neurosci. Methods *291*, 83–94.

143. Eom, M., Han, S., Park, P., Kim, G., Cho, E.-S., Sim, J., Lee, K.-H., Kim, S., Tian, H., Böhm, U.L., et al. (2023). Statistically unbiased prediction enables accurate denoising of voltage imaging data. Nat. Methods *20*, 1581–1592. https://doi.org/10.1038/s41592-023-02005-8.

144. Mukamel, E.A., Nimmerjahn, A., and Schnitzer, M.J. (2009). Automated analysis of cellular signals from large-scale calcium imaging data. Neuron *63*, 747–760. https://doi.org/10.1016/j.neuron.2009.08.009.

145. Xie, M.E., Adam, Y., Fan, L.Z., Böhm, U.L., Kinsella, I., Zhou, D., Rozsa, M., Singh, A., Svoboda, K., Paninski, L., et al. (2021). High-fidelity estimates of spikes and subthreshold waveforms from 1-photon voltage imaging in vivo. Cell Rep. *35*, 108954. https://doi.org/10.1016/j.celrep.2021.108954.

146. Chen, T.-W., Huang, X.-B., Plutkis, S.E., Holland, K.L., Lavis, L.D., and Lin, B.-J. (2025). Imaging neuronal voltage beyond the scattering limit. Nat. Methods *22*, 1366–1375. https://doi.org/10.1038/s41592-025-02692-5.

147. Schneider, S., Lee, J.H., and Mathis, M.W. (2023). Learnable latent embeddings for joint behavioural and neural analysis. Nature *617*, 360–368. https://doi.org/10.1038/s41586-023-06031-6.

148. Stringer, C., and Pachitariu, M. (2024). Analysis methods for large-scale neuronal recordings. Science *386*, eadp7429. https://www.science.org/doi/full/10.1126/science.adp7429.

149. Langdon, C., Genkin, M., and Engel, T.A. (2023). A unifying perspective on neural manifolds and circuits for cognition. Nat. Rev. Neurosci. *24*, 363–377. https://doi.org/10.1038/s41583-023-00693-x.

150. Inagaki, S., Nakagawa-Tamagawa, N., Huynh, N.Z., Kambe, Y., Yagasaki, R., Manita, S., Fujimoto, S., Noda, T., Mori, M., Teranishi, A., et al. (2026). Isotonic and minimally invasive optical clearing media for live cell imaging ex vivo and in vivo. Nat. Methods *23*, 839–853. https://doi.org/10.1038/s41592-026-03023-y.